Spin-State Switching: Chemical Modulation and the Impact of Intermolecular Interactions in Manganese(III) Complexes

Sukanya Bagchi,[†] *Sujit Kamilya*,[†] *Sakshi Mehta,*[†] *Subhankar Mandal*,[†] *Arka Bandyopadhyay*,[†] *Awadhesh Narayan*,[†] *Subrata Ghosh,*[*,†] *and Abhishake Mondal*[*,†]

[†]*Solid State and Structural Chemistry Unit, Indian Institute of Science, Sir C V Raman Road, Bangalore 560012, India.*

Email: subratagchem@gmail.com; mondal@iisc.ac.in

Table of Content:

Experimental Section

Materials and physical measurements

All manipulations were carried out under air unless otherwise stated. Solvents were dried by standard methods and freshly distilled before use. All chemicals were used as purchased from chemical sources without further purification. The crystals of complexes were removed from the mother liquor and dried on filter paper to remove any adhering solvent molecules, prior to measurement. The elemental analyses of C, H and N were performed with Thermo Scientific Flash 2000 Organic Elemental Analyzer. Infrared (IR) spectra were recorded in the range of 4000 – 500 cm^{-1} on the Perkin Elmer spectrometer. UV-vis-NIR spectra were carried out in the region of 250 – 2000 nm on a Lambda 1050+ UV-vis-NIR spectrometer. The UV-vis spectroscopic measurements in solution were performed in quartz cuvettes with path length of 1 cm. Solid-state measurements were carried out by taking 5% sample by weight in KBr. Thermogravimetric analysis (TGA) was done on a Mettler Toledo TGA/SDTA851 analyzer with a heating rate of 10 K min^{-1} under a nitrogen atmosphere ranging from 300 K to 573 K. Differential scanning calorimetry (DSC) measurements were performed using Mettler Toledo DSC 823^e differential scanning calorimeter with a scan rate of 10 K min^{-1} and 5 K min^{-1} in a nitrogen atmosphere. Powder X-ray diffraction (PXRD) measurements were carried out on a PANalytical Empyrean diffractometer at 45 kV and 30 mA, under Cu-Kα radiation (λ = 1.54059 Å). PXRD data analyses were done using PANalytical X'Pert HighScore Plus software.[1] Electrochemistry experiments were performed with a Metrohm Autolab PGSTAT101 using platinum as working electrode in acetonitrile with 0.2 M (^{n}Bu$_4$)NPF$_6$ as supporting electrolyte. Ferrocene was used as an internal reference.

Magnetic Measurements

The magnetic susceptibility measurements were carried out with Quantum Design MPMS-XL EverCool SQUID magnetometer, between 2 and 300 K for dc applied fields ranging from -5 T to

5 T for **1** - **5**. Polycrystalline samples of **1** - **5** (17.24, 19.66, 20.09, 22.50, and 23.46 mg, respectively) introduced in a polyethylene bag (2.8 × 0.75 × 0.02 cm) were subjected to measurements. The temperature dependent data were measured using 1000 Oe dc fields. The isothermal magnetization data were acquired at 2, 5 and 6 K. *M vs H* measurements were performed at 100 K to check for the presence of ferromagnetic impurities which were found to be absent. The magnetic data were corrected for the sample holder and the diamagnetic contribution.

X-ray crystallography

Single−crystal X−ray diffraction studies of complexes **1** – **5** were performed with a Bruker SMART APEX CCD diffractometer equipped with graphite−monochromated Mo Kα radiation (λ = 0.71073 Å). The single crystal was mounted on a crystal mounting loop with the help of Paratone oil at 296 K and slowly cooled down to the measured temperature with a 2 K/min ramping rate using a liquid nitrogen gas-stream cooling device, followed by data collection at respective temperatures. Data integration and reduction were carried out using SAINT software, and empirical absorption corrections were performed using the SADABS program.[2] Structures were solved using direct methods and refined with a full-matrix least-squares method on F^2 using SHELXL-2018 included in OLEX 2 version 1.3.0.[3] The disordered water molecule present in the crystal structure of complex **4** was masked by using SOLVENT MASK procedure in OLEX 2 which is equivalent to SQUEEZE in PLATON. The void space (55 $Å^3$) and number of electrons (11) confirm the presence of one water molecule per asymmetric unit which accounts for four water molecules per unit cell. The packing diagrams were made using Mercury 4.2.0.[4]

All other non-hydrogen atoms of complexes **1** - **5** were refined anisotropically and hydrogen atoms were labeled to ideal positions and refined isotropically using a riding model. CCDC 2238253 – 2238257 and 2238260 - 2238263 contain the supplementary crystallographic data for

this paper. These data can be obtained free of charge from The Cambridge Crystallographic Data Centre via www.ccdc.cam.ac.uk/data_request/cif..

Figures

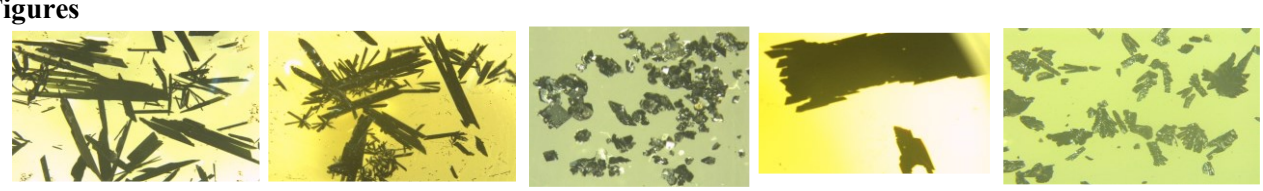

Fig. S1. Picture of crystals for complexes **1 – 5** (left to right).

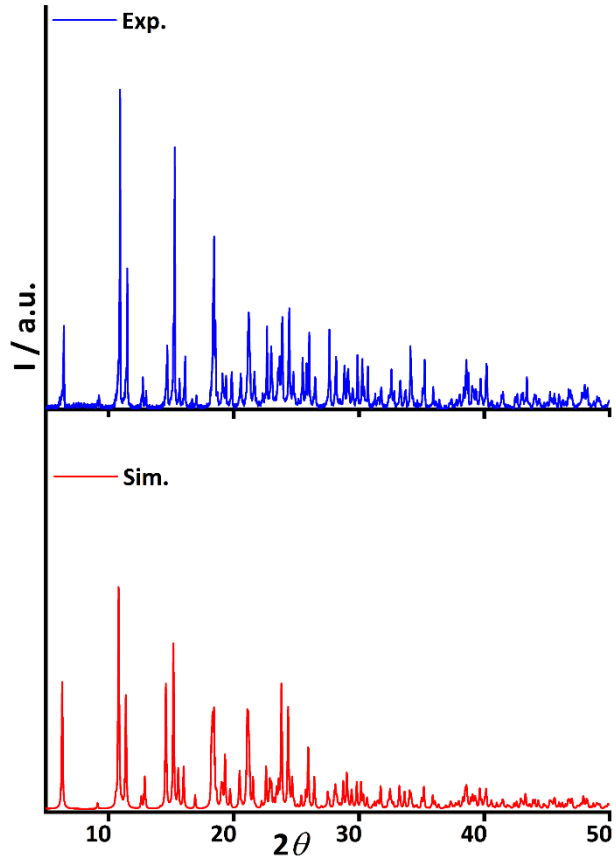

Fig. S2. Comparison of the room temperature experimental PXRD pattern and the 296 K simulated one for **1**.

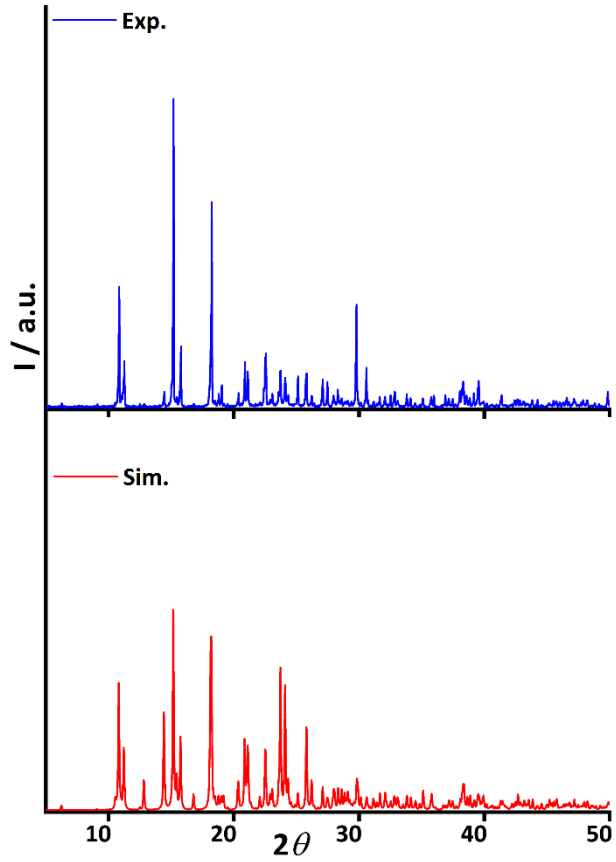

Fig. S3. Comparison of the room temperature experimental PXRD pattern and the 296 K simulated one for **2**.

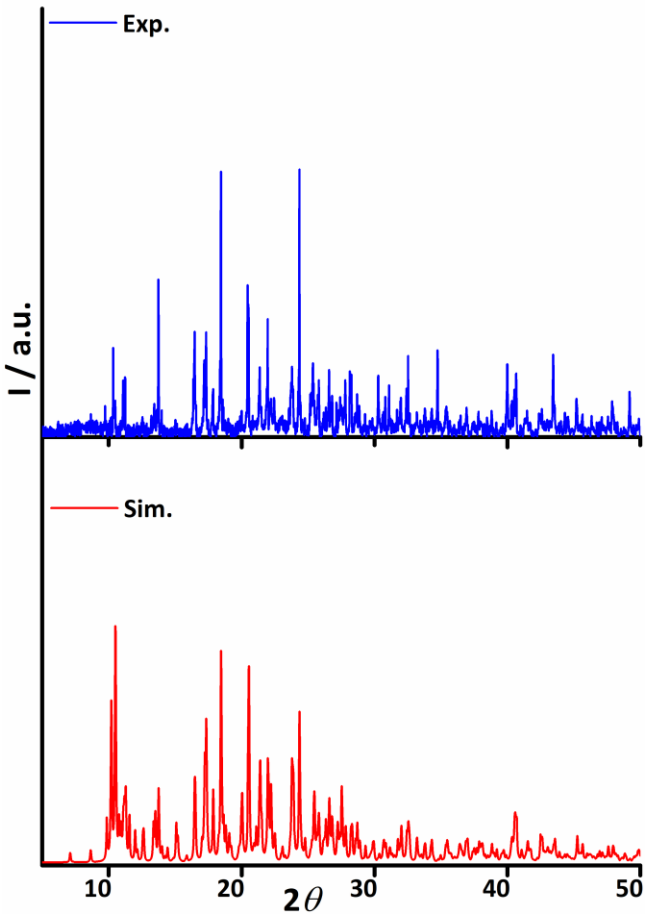

Fig. S4. Comparison of the room temperature experimental PXRD pattern and the 296 K simulated one for **3**.

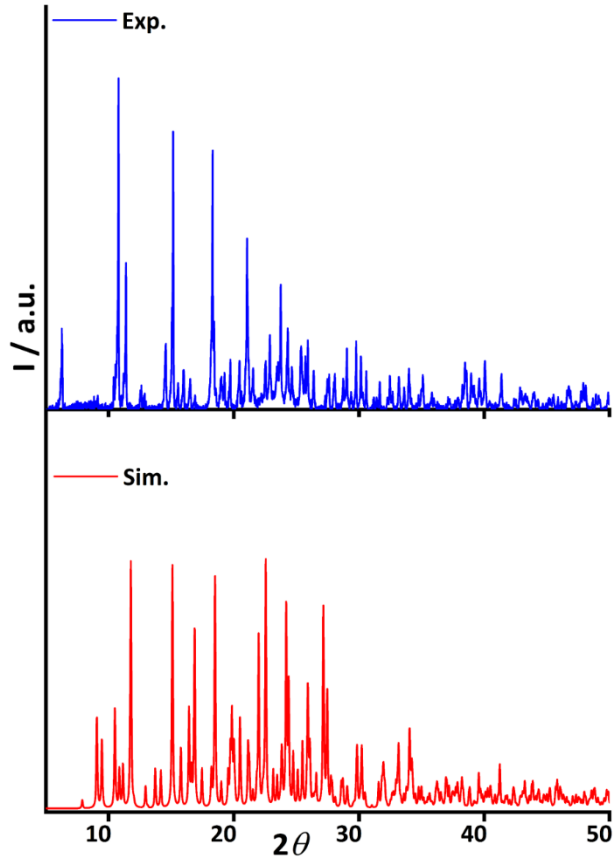

Fig. S5. Comparison of the room temperature experimental PXRD pattern and the 296 K simulated one for **4**.

The reason for the slight deviation in the experimental PXRD data for complex **4** is probably due to the partial solvent loss during the sample preparation for the PXRD measurement at room temperature.

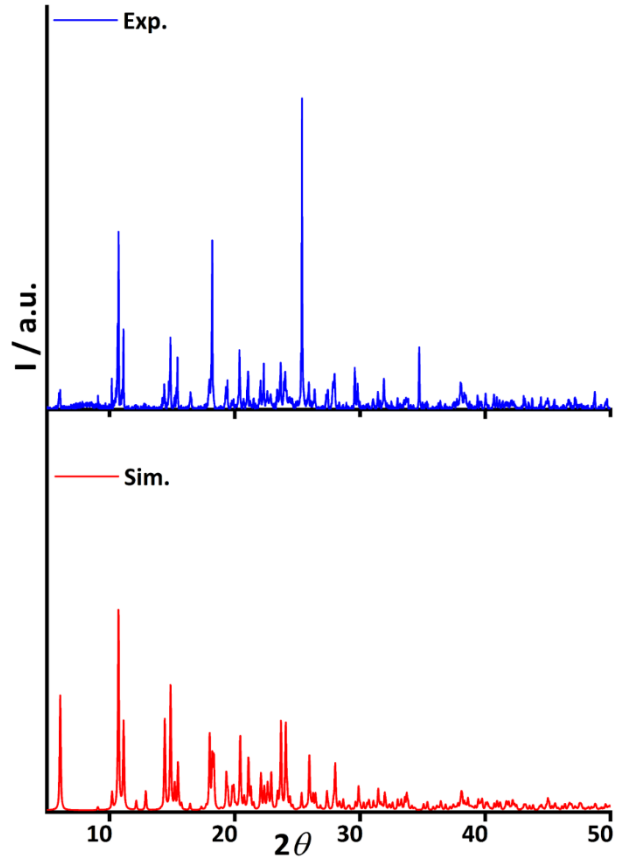

Fig. S6. Comparison of the room temperature experimental PXRD pattern and the 296 K simulated one for **5**.

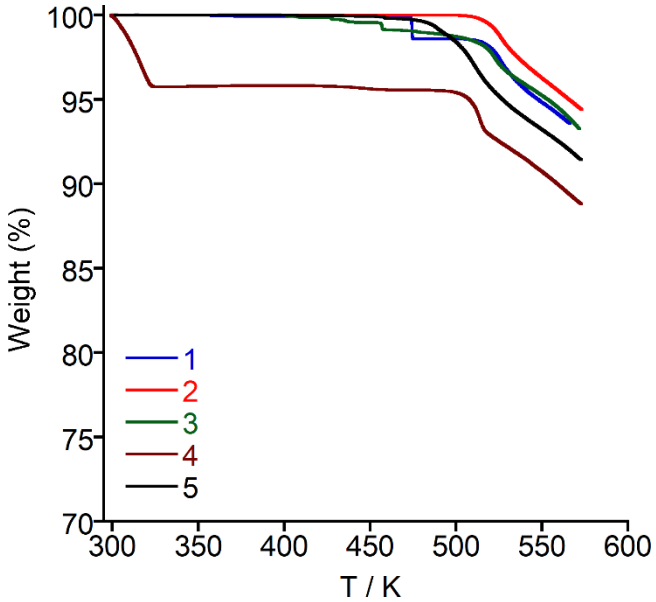

Fig. S7. Thermogravimetric analysis (TGA) for **1 – 5** from 303 K to 573 K temperature range at 10 K min^{-1} sweep rate under N_2 atmosphere.

Complexes **1** – **5** were characterized fully by solid-state IR spectroscopy at room temperature (Fig. S8). The IR spectra display the characteristic C=N and N–H stretching vibrations of coordinated Schiff-base ligand at around 1620 – 1625 cm^{-1} and 3225 – 3240 cm^{-1} respectively while the bands around 915 and 850 cm^{-1} suggested the presence of ReO_4^- anion in all these complexes. In addition, IR spectra show typical absorption of the coordinated Schiff-base ligands at around 1595, 1540, 1460, 1423, 1370, 1280, 1072, 1048, 860, 705 and 560 cm^{-1}.

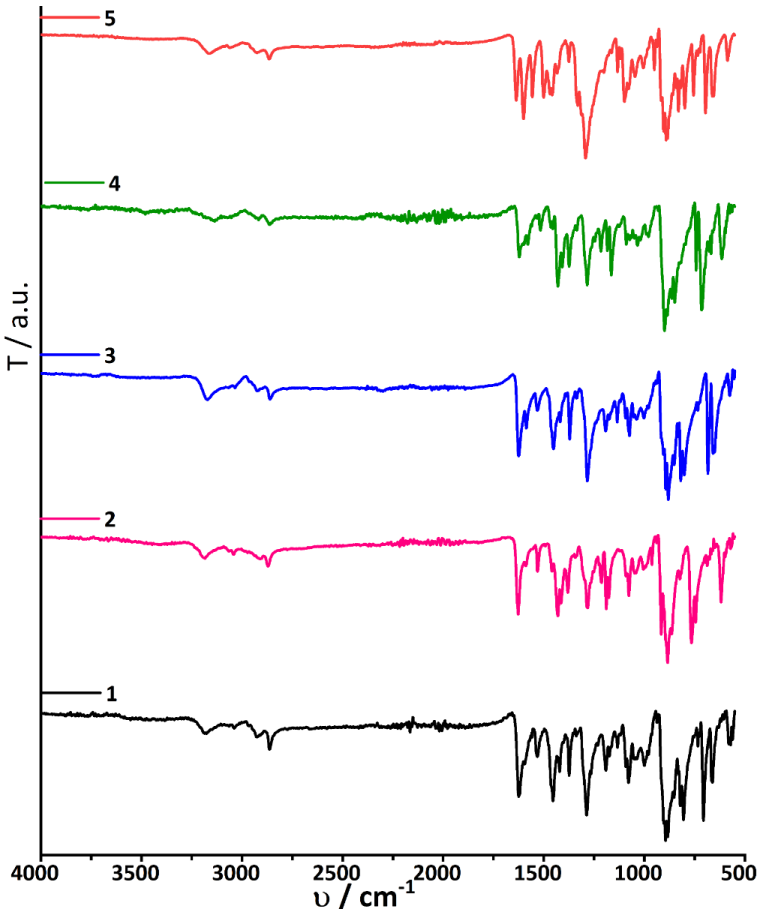

Fig. S8. ATR IR spectra of **1** – **5** at room temperature.

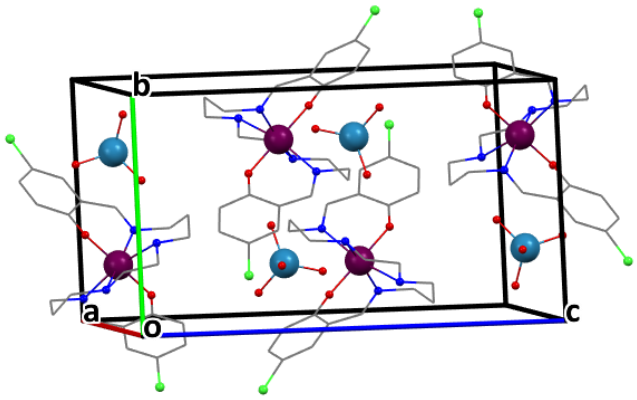

Fig. S9. Perspective view of unit cell in **1** at 296 K. Hydrogen atoms are omitted for clarity (Mn: Purple, C: gray, N: blue, O: red, Cl: green, Re: teal blue).

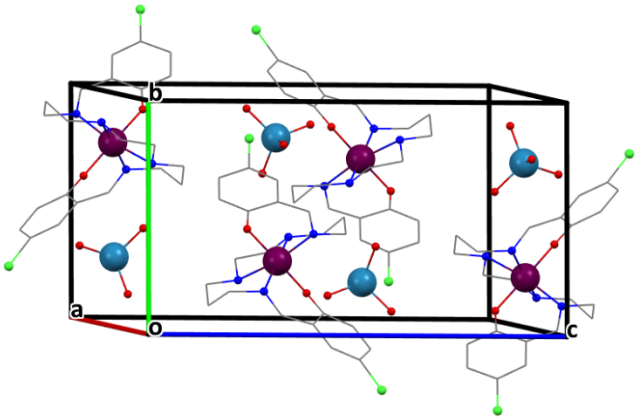

Fig. S10. Perspective view of unit cell in **1** at 120 K. Hydrogen atoms are omitted for clarity (Mn: Purple, C: gray, N: blue, O: red, Cl: green, Re: teal blue).

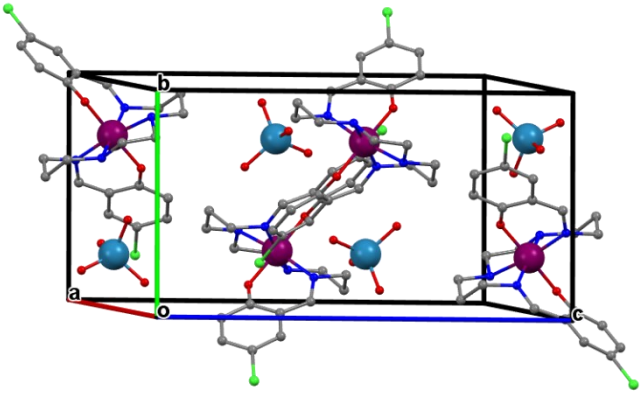

Fig. S11. Perspective view of unit cell in **1** at 90 K. Hydrogen atoms are omitted for clarity (Mn: Purple, C: gray, N: blue, O: red, Cl: green; Re: teal blue).

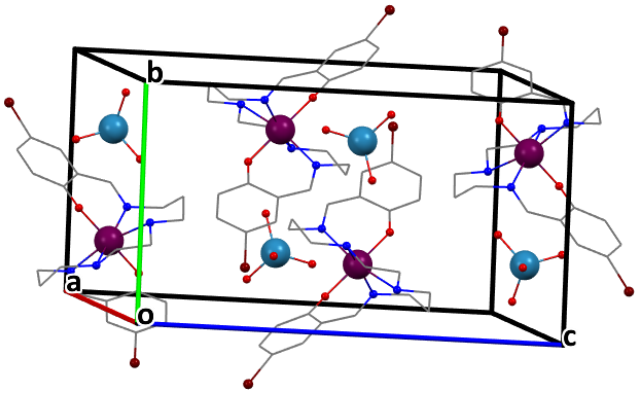

Fig. S12. Perspective view of unit cell in **2** at 296 K. Hydrogen atoms are omitted for clarity (Mn: Purple, C: gray, N: blue, O: red, Br: brown, Re: teal blue).

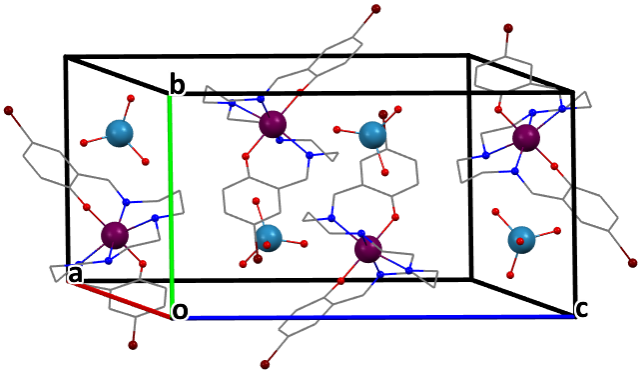

Fig. S13. Perspective view of unit cell in **2** at 120 K. Hydrogen atoms are omitted for clarity (Mn: Purple, C: gray, N: blue, O: red, Br: brown, Re: teal blue).

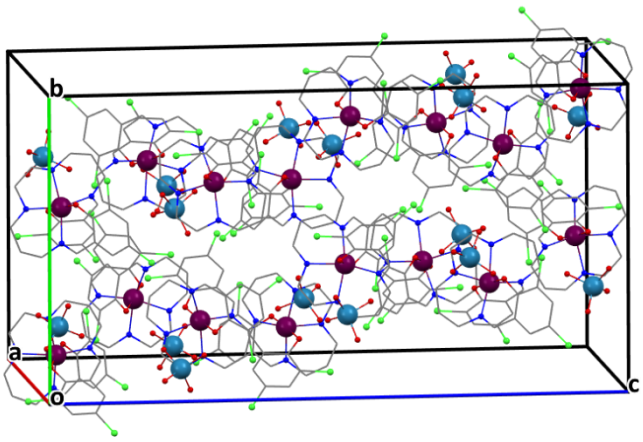

Fig. S14. Perspective view of unit cell in **3** at 296 K. Hydrogen atoms are omitted for clarity (Mn: Purple, C: gray, N: blue, O: red, Cl: green, Re: teal blue).

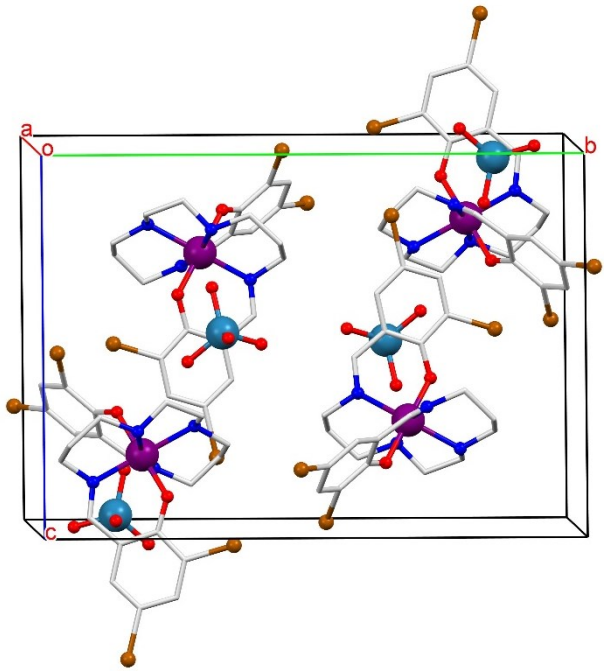

Fig. S15. Perspective view of unit cell in **4** at 296 K. Hydrogen atoms are omitted for clarity (Mn: Purple, C: gray, N: blue, O: red, Br: brown, Re: teal blue).

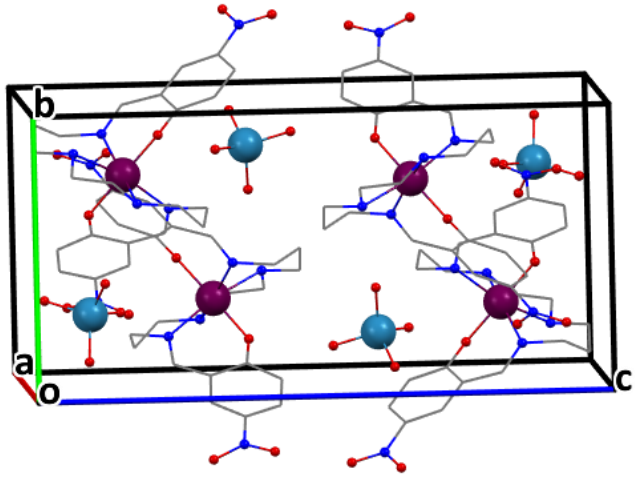

Fig. S16. Perspective view of unit cell in **5** at 296 K. Hydrogen atoms are omitted for clarity (Mn: Purple, C: gray, N: blue, O: red, Re: teal blue).

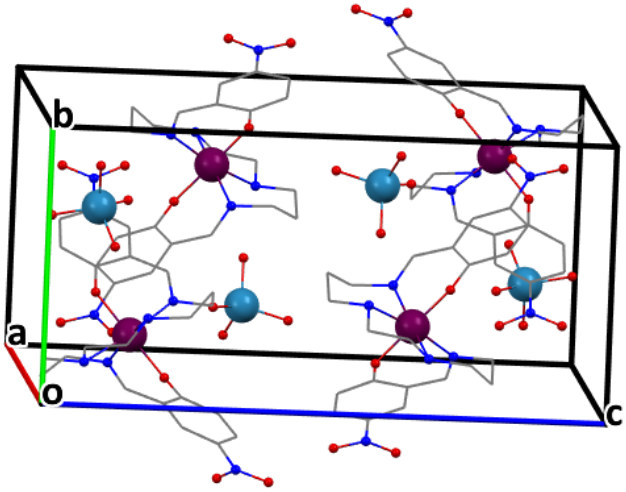

Fig. S17. Perspective view of unit cell in **5** at 120 K. Hydrogen atoms are omitted for clarity (Mn: Purple, C: gray, N: blue, O: red, Re: teal blue).

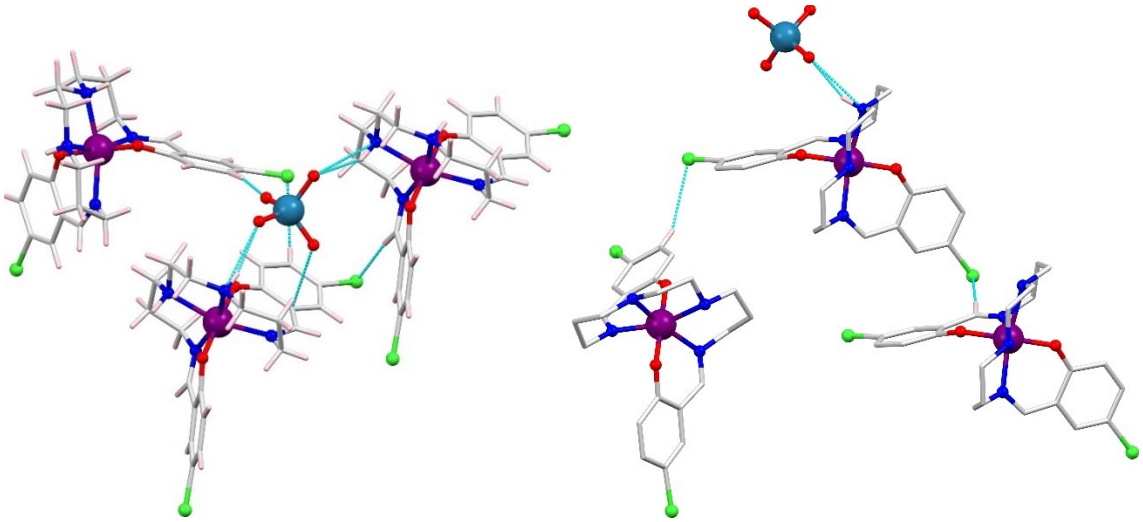

Fig. S18. Perspective view of a fragment of the supramolecular structure displaying several weak interactions (cyan lines) coming from ReO_4^- counter anion (left) and Cl atoms (right) in **1** at 296 K.

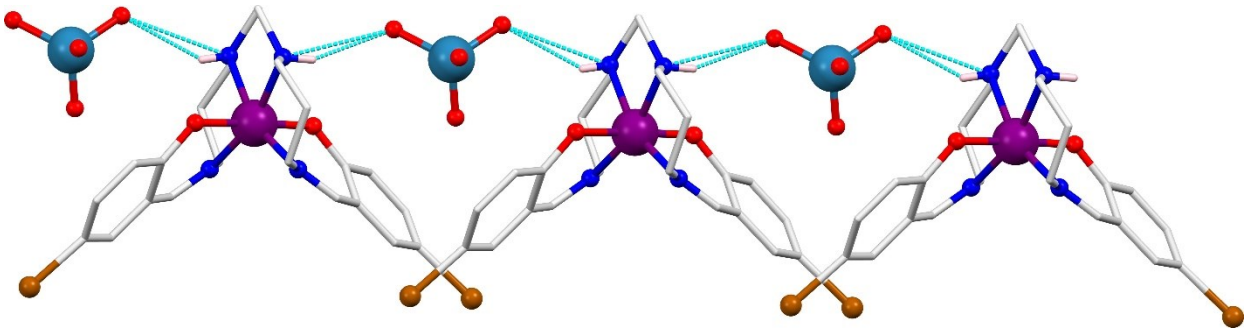

Fig. S19. View of N–H···O interactions (cyan lines) forming 1D chain in **2** at 296 K.

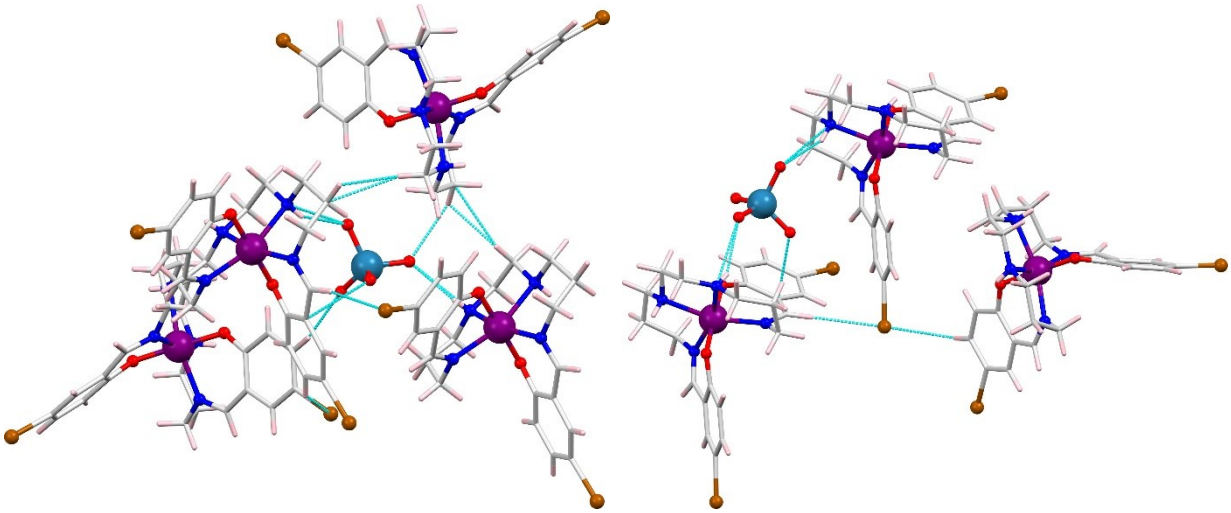

Fig. S20. Perspective view of a fragment of the supramolecular structure displaying several weak interactions (cyan lines) coming from ReO_4^- counter anion (left) and Br atom (right) in **2** at 296 K.

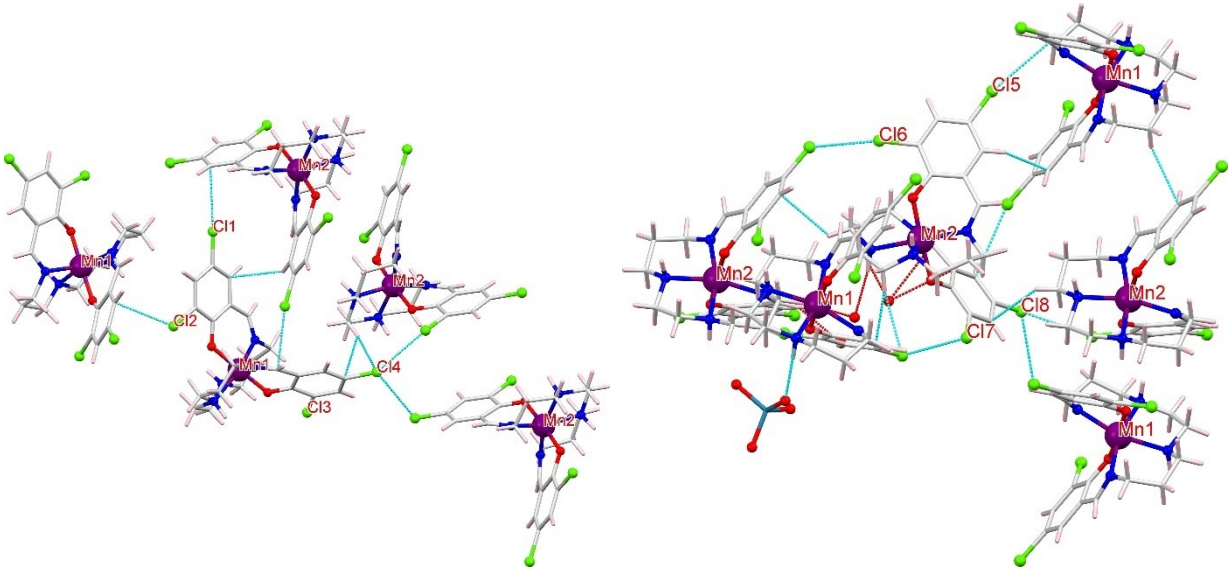

Fig. S21. Perspective view of a fragment of the supramolecular structure displaying several weak interactions (cyan lines) coming from Cl atom in **3** at 296 K.

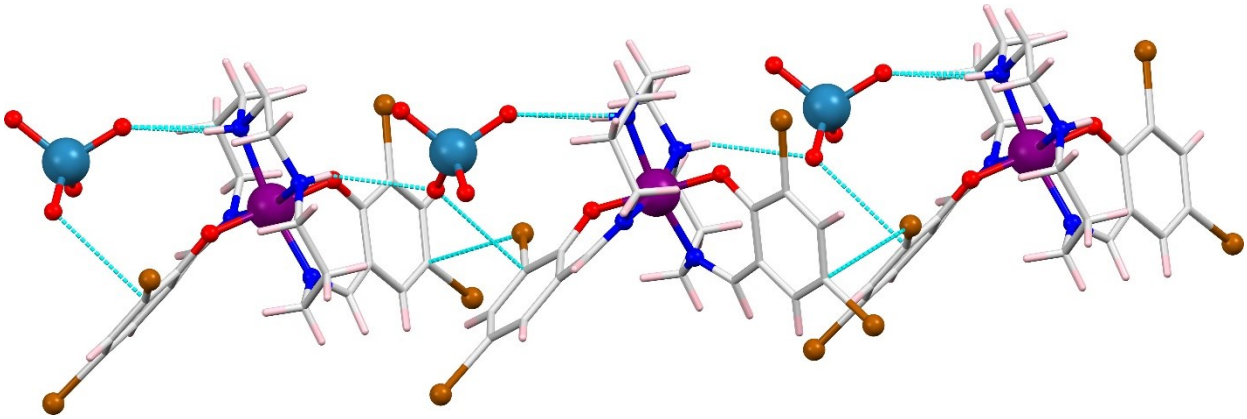

Fig. S22. View of N–H···O interactions (cyan lines) forming 1D chain in **4** at 296 K.

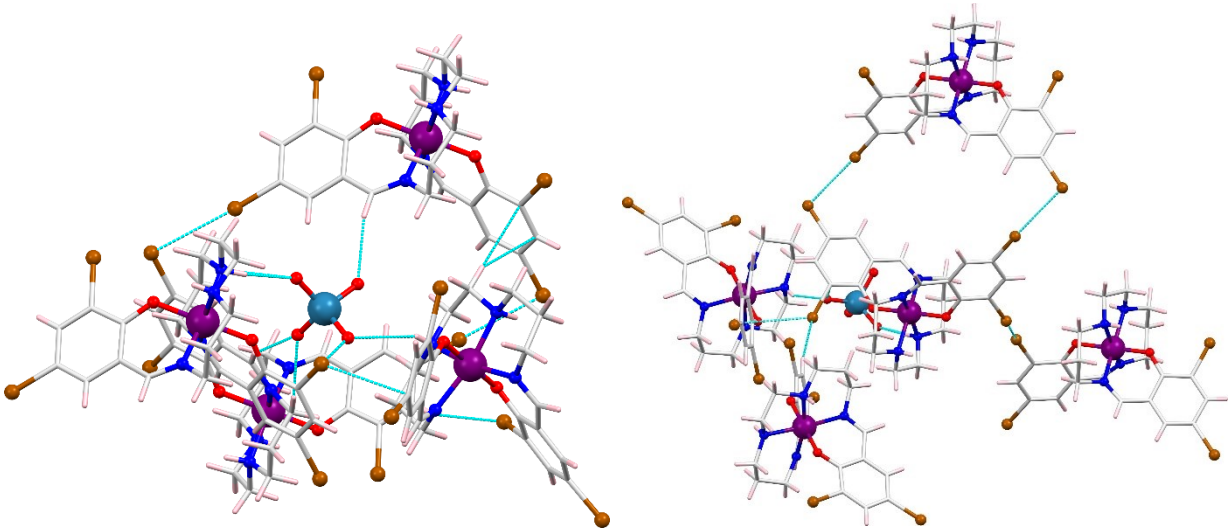

Fig. S23. Perspective view of a fragment of the supramolecular structure displaying several weak interactions (cyan lines) coming from ReO_4^- counter anion (left) and Br atoms (right) in **4** at 296 K.

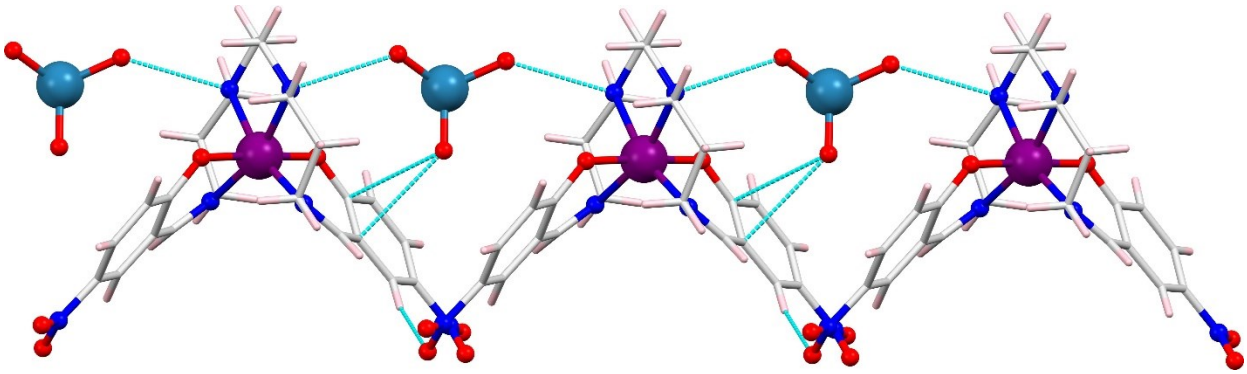

Fig. S24. View of N–H···O interactions (cyan lines) forming 1D chain in **5** at 296 K.

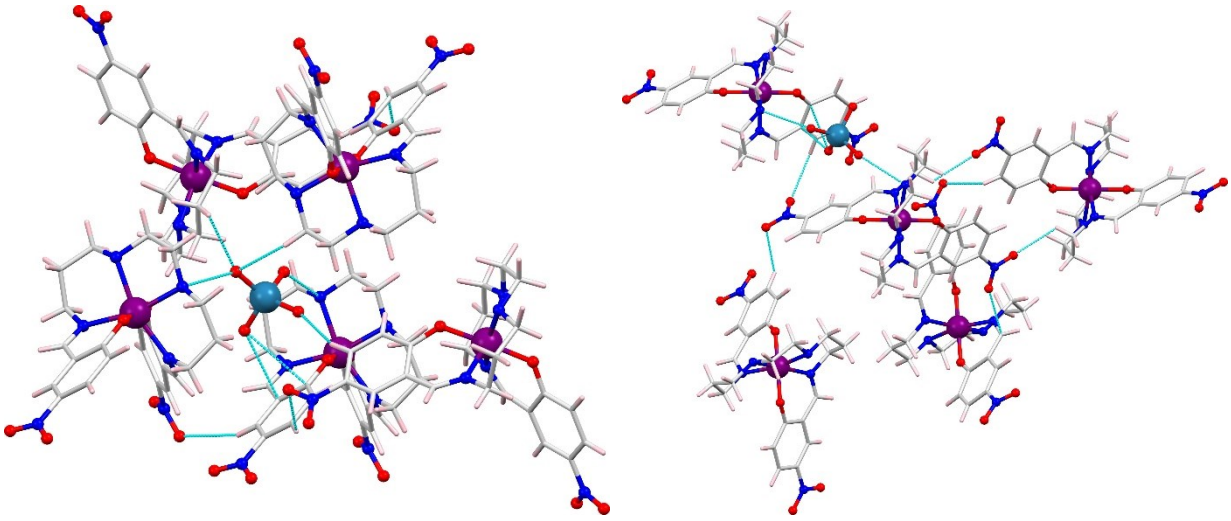

Fig. S25. Perspective view of a fragment of the supramolecular structure displaying several weak interactions (cyan lines) coming from ReO_4^- counter anion (left) and NO_2 group (right) in **5** at 296 K.

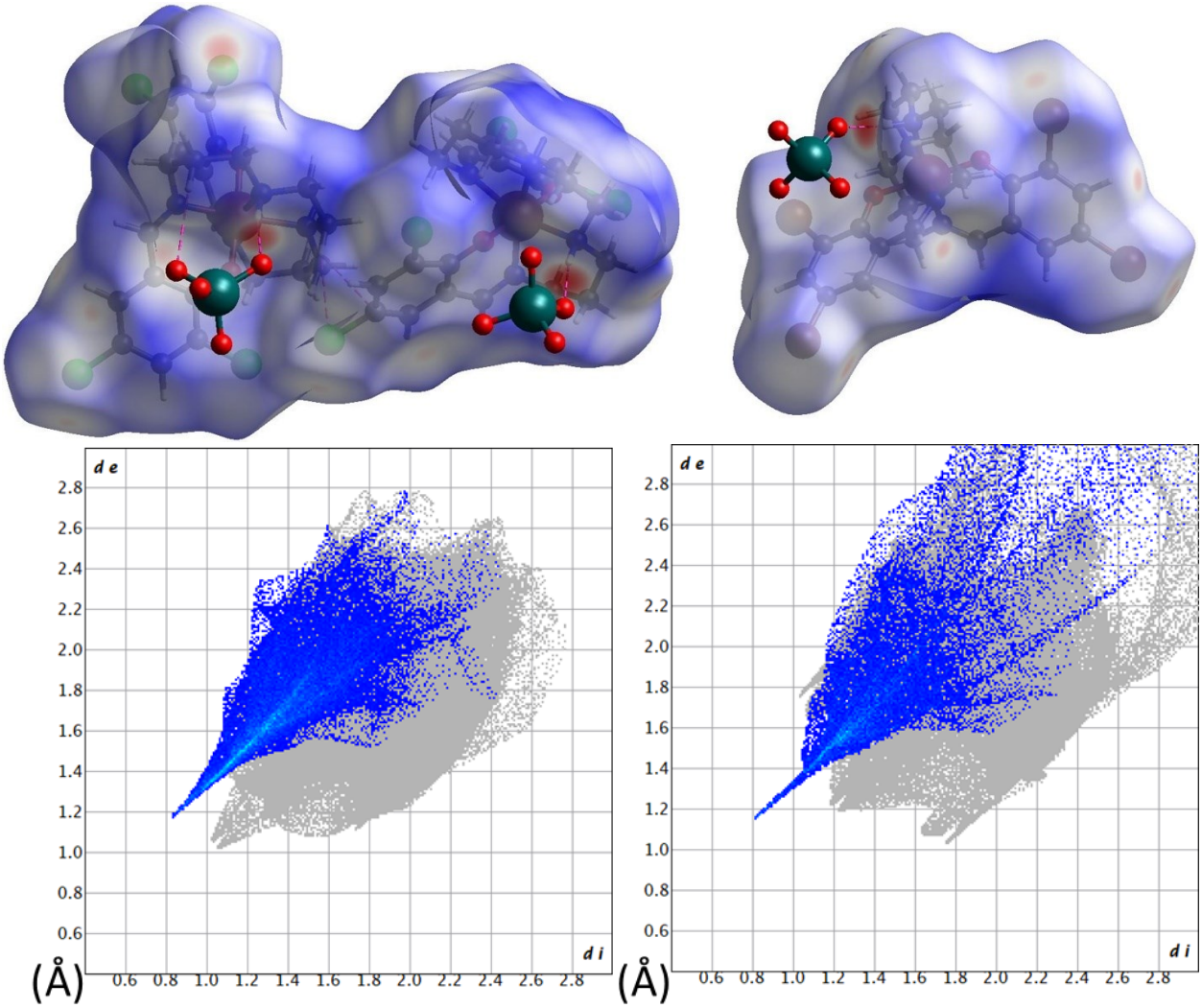

Fig. S26. Hirshfeld surface analysis of complexes **3** (left) and **4** (right), showing the d_{norm} surfaces of the monocationic unit ([Mn(5X-sal$_2$-323)]$^+$) (top) and 2D fingerprint plots of O···H contact (bottom) at 296 K.

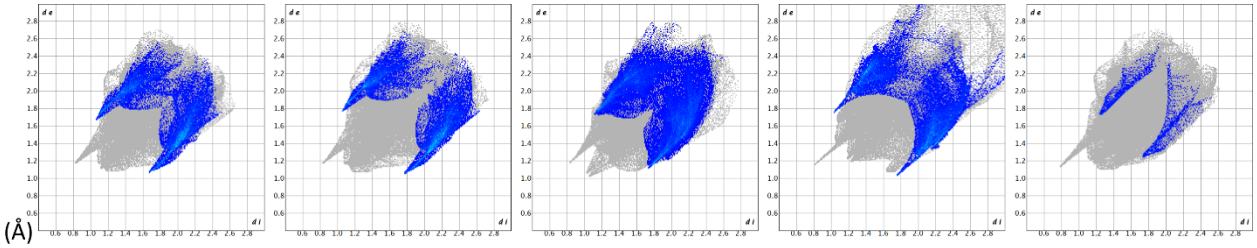

Fig. S27. Hirshfeld surface analysis of complexes **1** - **5** (left to right), showing 2D fingerprint plots of X···H contacts at 296 K.

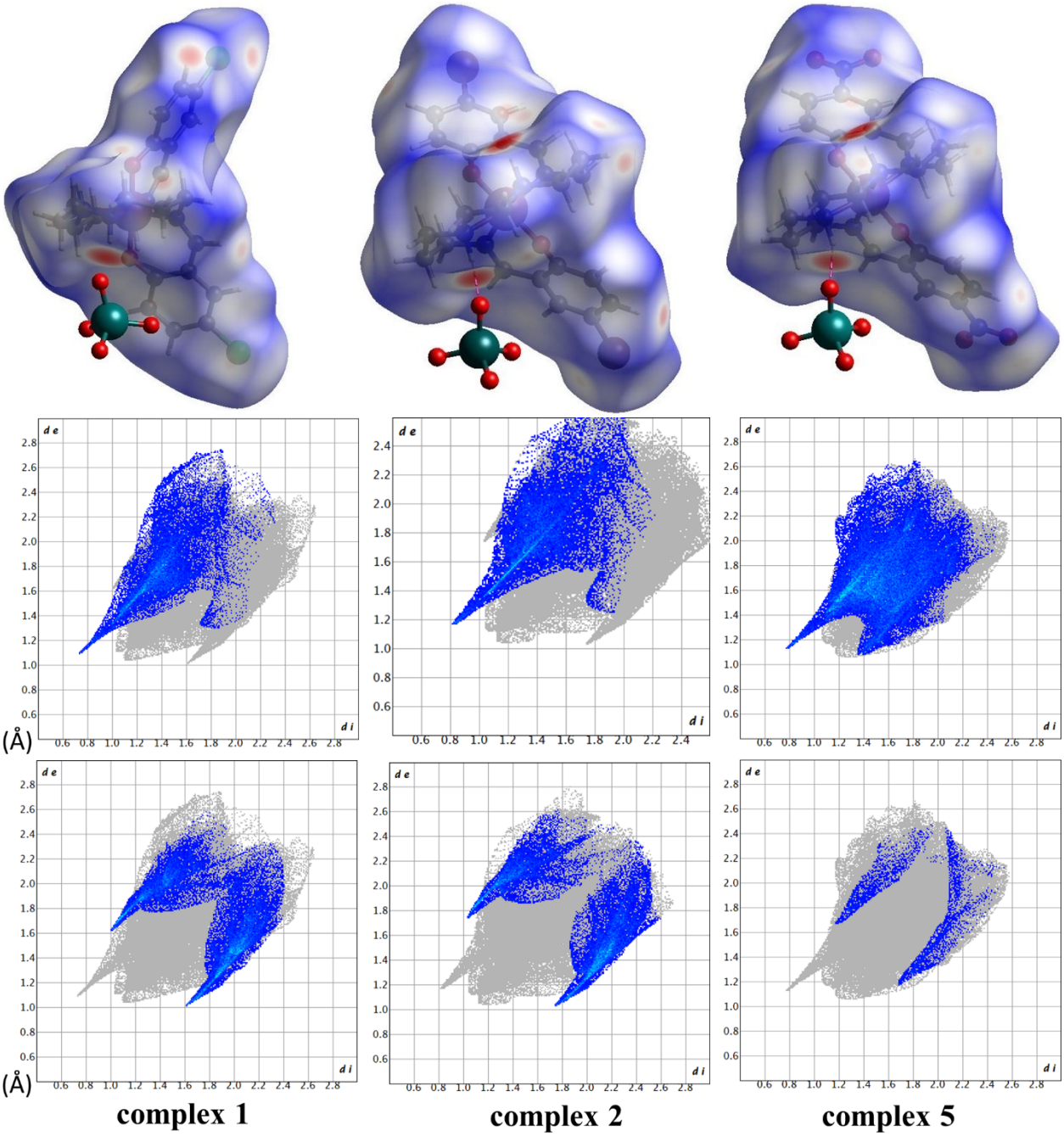

Fig. S28. Hirshfeld surface analysis of complexes **1**, **2**, and **5** (left to right), showing the d_{norm} surfaces of the monocationic unit ([Mn(5X-sal$_2$-323)]$^+$) (top) and 2D fingerprint plots of O···H contact (middle) and X···H contact (bottom) at 90 K for **1** and 120 K for **2** and **5**.

Spectroscopic studies

UV-vis-NIR spectroscopic studies were carried out on **1** – **5** in solid-state as well as in solution at room temperature (Fig. S29 and S30). UV-vis-NIR spectra of **1** – **3**, and **5** in acetonitrile exhibit one broad band along with two shoulders at around 1179 – 1275 nm, 660 – 687 nm, and 580 – 601 nm respectively, which are ascribed to the *d-d* transitions ($^5A_{1g} \rightarrow {}^5B_{1g}$, $^5A_{1g} \rightarrow {}^5E_g$ and $^5A_{1g} \rightarrow {}^5B_{2g}$) for HS manganese(III) ion in a distorted octahedral system which is tetragonally compressed. Due to the tailing effect from the nearby ligand-to-metal charge transfer (LMCT) transition the band around 580 – 601 nm has a higher molar coefficient. However, the UV-vis-NIR spectrum of **4** exhibited a broad band at around 1276 nm, a bulge at 693 nm, and a sharp band at around 597 nm, which may be attributed to the *d-d* transitions for LS manganese(III). Apart from the *d-d* transitions, UV-vis-NIR spectra reveal the phenolate ligand-based LMCT transition at around 520 – 537 nm, LMCT transition from imine and amine-based nitrogen donors around 369 - 380 nm, and intra-ligand charge transfer (ILCT) transition at around 271 – 288 nm. The solid-state spectra of complexes **1** – **5** also exhibit very similar absorption bands suggesting that all complexes have well-preserved its identity in both solid-state as well as upon dissolution.

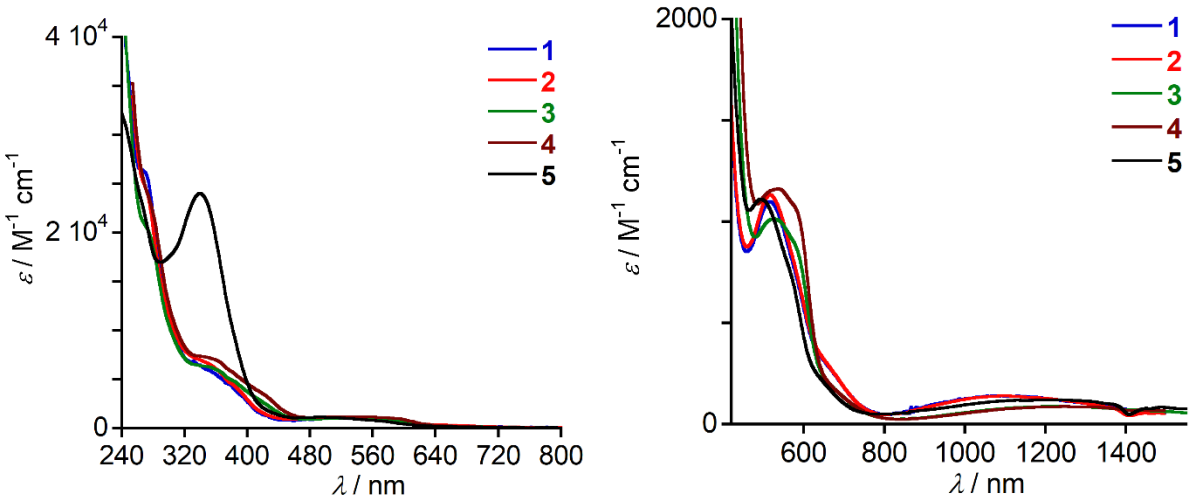

Fig. S29. UV-vis-NIR spectra of **1** – **5** in MeCN with dilute (left) and concentrated (right) solutions at room temperature.

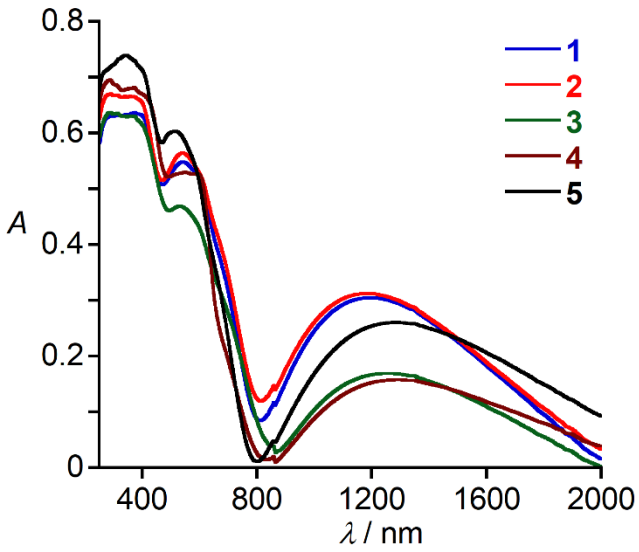

Fig. S30. Solid state UV-vis-NIR spectra of **1** – **5** in KBr at room temperature.

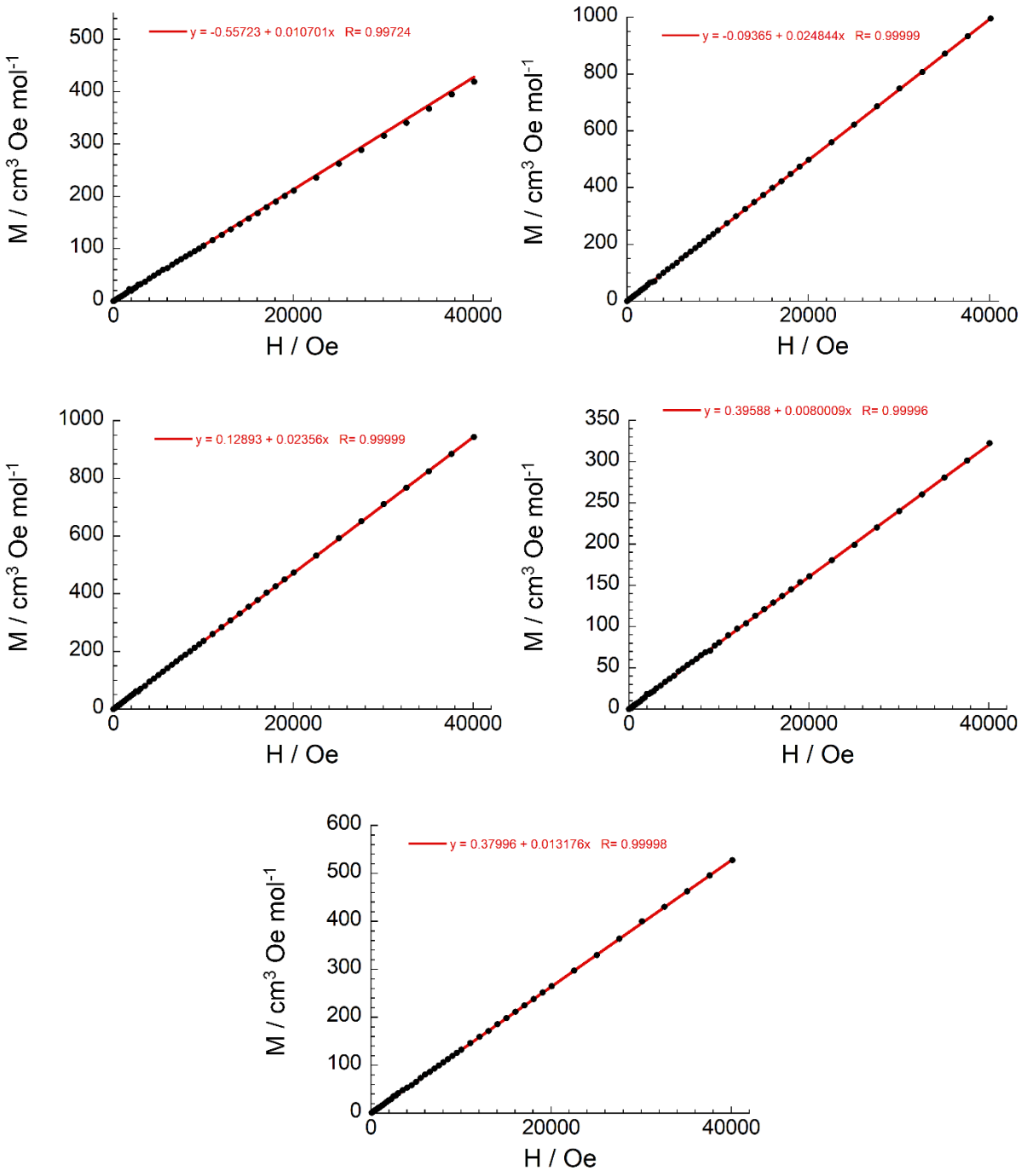

Fig. S31. Field dependence of the magnetization as *M vs H* plots for **1** - **5** at 100 K. The solid line is the best fit.

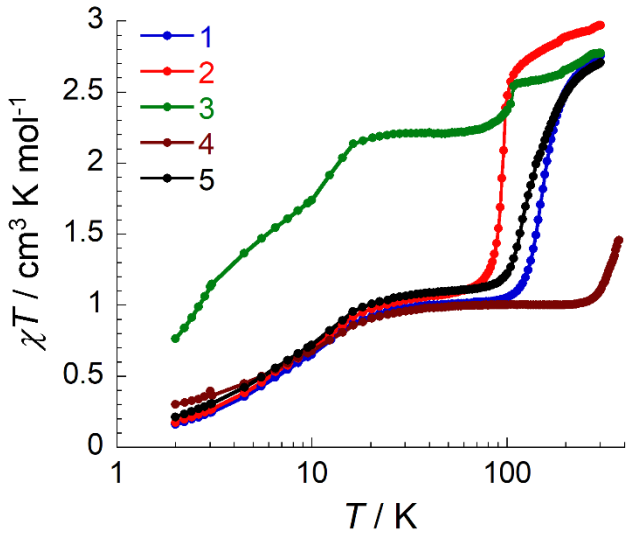

Fig. S32. Temperature dependence of χT product in log scale for **1** – **5** at 1000 Oe.

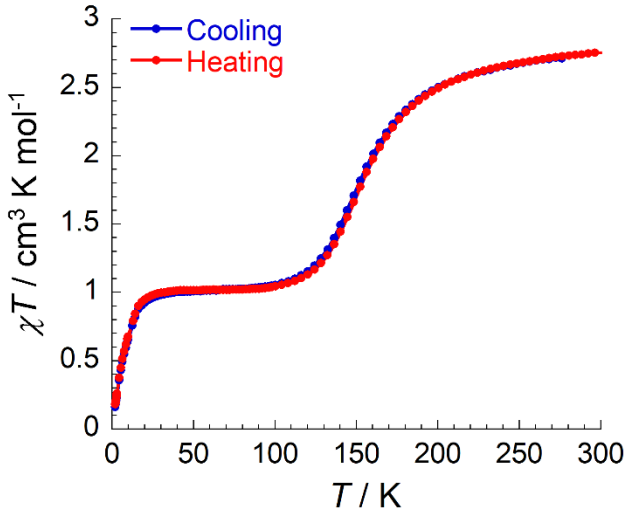

Fig. S33. Temperature dependence of χT product for **1** at 1000 Oe in cooling and heating mode.

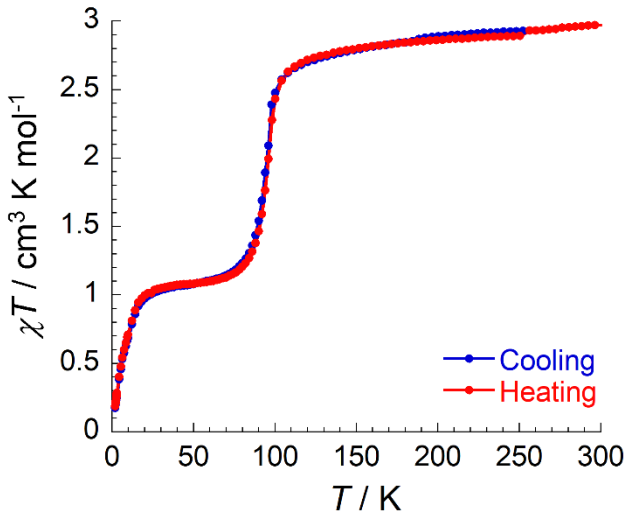

Fig. S34. Temperature dependence of χT product for **2** at 1000 Oe in cooling and heating mode.

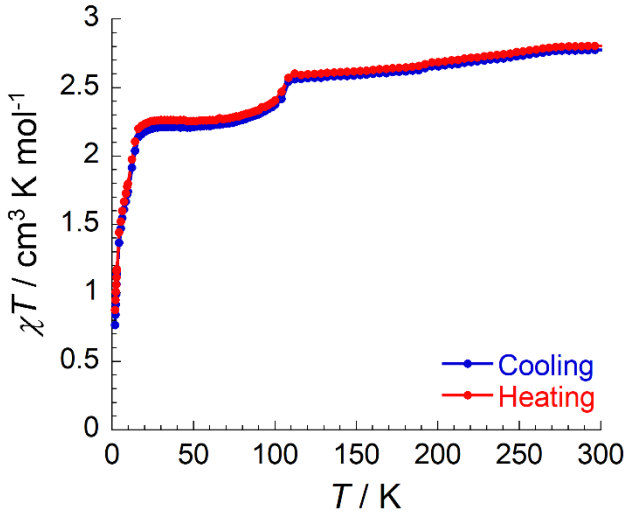

Fig. S35. Temperature dependence of χT product for **3** at 1000 Oe in cooling and heating mode.

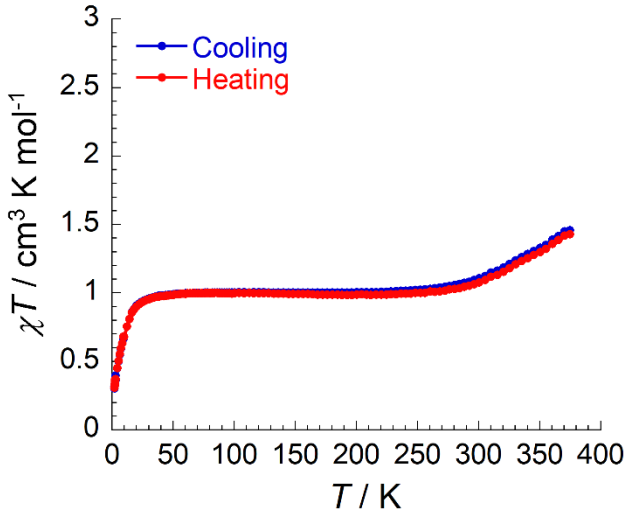

Fig. S36. Temperature dependence of χT product for **4** at 1000 Oe in cooling and heating mode.

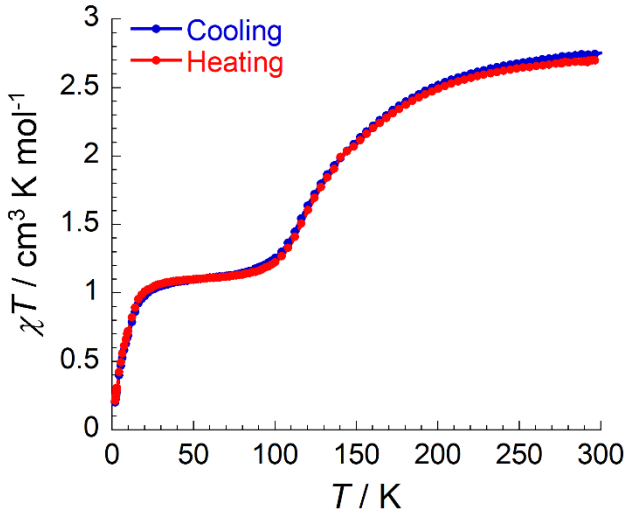

Fig. S37. Temperature dependence of χT product for **5** at 1000 Oe in cooling and heating mode.

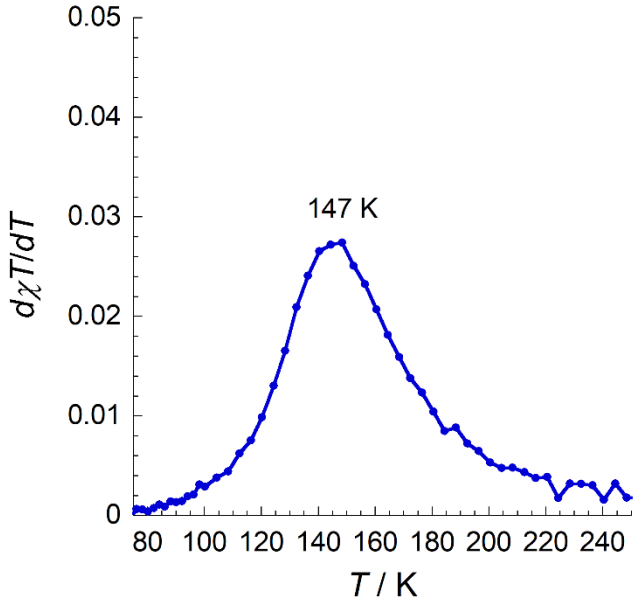

Fig. S38. The first derivative of χT against the temperature, dχT /dT *vs*. T, identifies $T_{1/2}$ = 147 K for **1**.

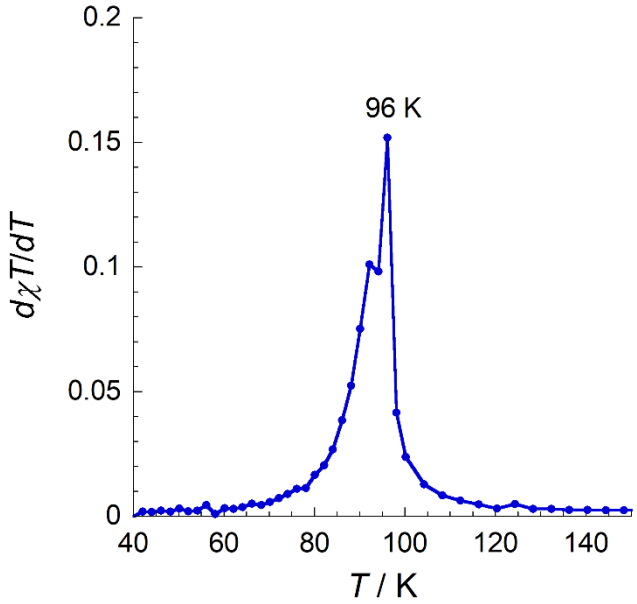

Fig. S39. The first derivative of χT against the temperature, dχT /dT *vs*. T, identifies $T_{1/2}$ = 96 K for **2**.

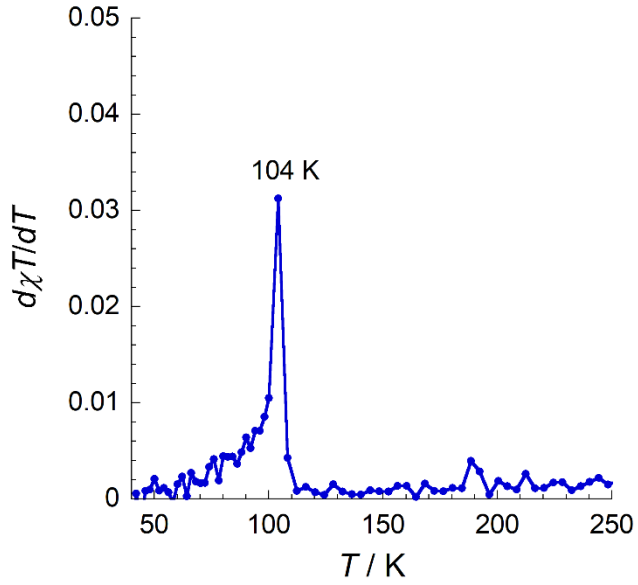

Fig. S40. The first derivative of χT against the temperature, dχT /dT *vs*. T, identifies $T_{1/2}$ = 104 K for **3**.

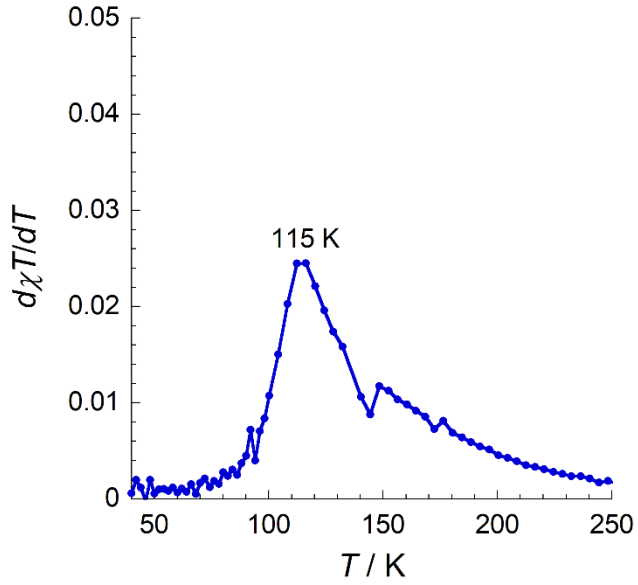

Fig. S41. The first derivative of χT against the temperature, dχT /dT *vs*. T, identifies $T_{1/2}$ = 115 K for **5**.

The following equation deduced from the ideal solution model was applied to fit the spin crossover properties observed by magnetic studies.

$$X = X_{LS} + \frac{X_{HS} - X_{LS}}{1 + \exp\left[\Delta H/R\,(1/T - 1/T_{1/2})\right]}$$

X = χT product

X_{LS} = χT product for pure low-spin

X_{HS} = χT product for pure high-spin

ΔH = Enthalpy change associated with the spin crossover phenomenon

R = Ideal gas constant

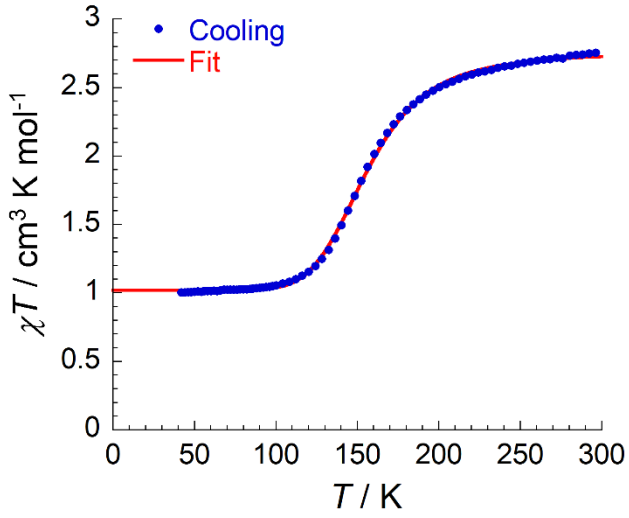

Fig. S42 Fitting of χT *vs* T data of **1** using the ideal solution model.

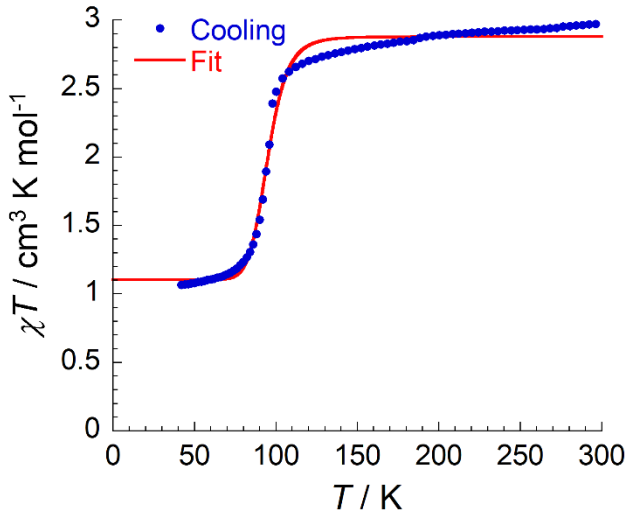

Fig. S43 Fitting of χT *vs* T data of **2** using the ideal solution model.

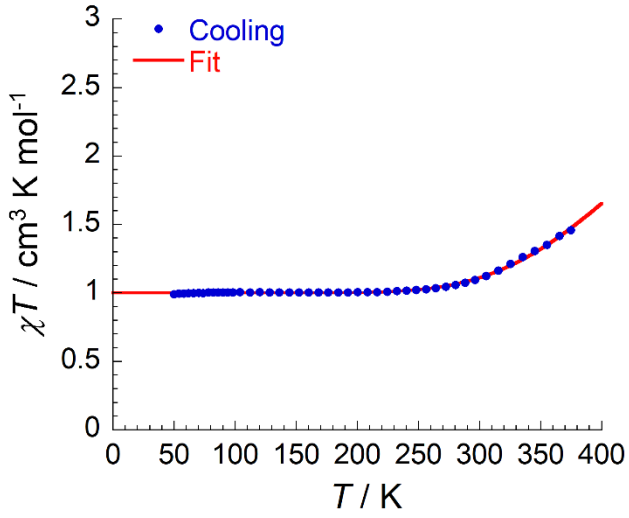

Fig. S44 Fitting of χT *vs* T data of **4** using the ideal solution model.

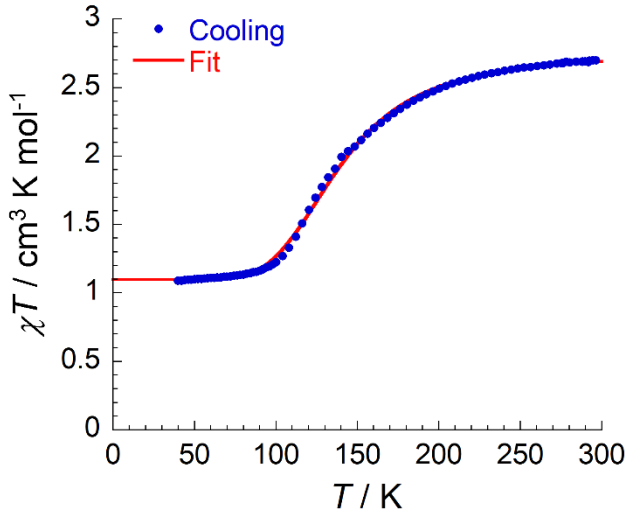

Fig. S45 Fitting of χT *vs* T data of **5** using the ideal solution model.

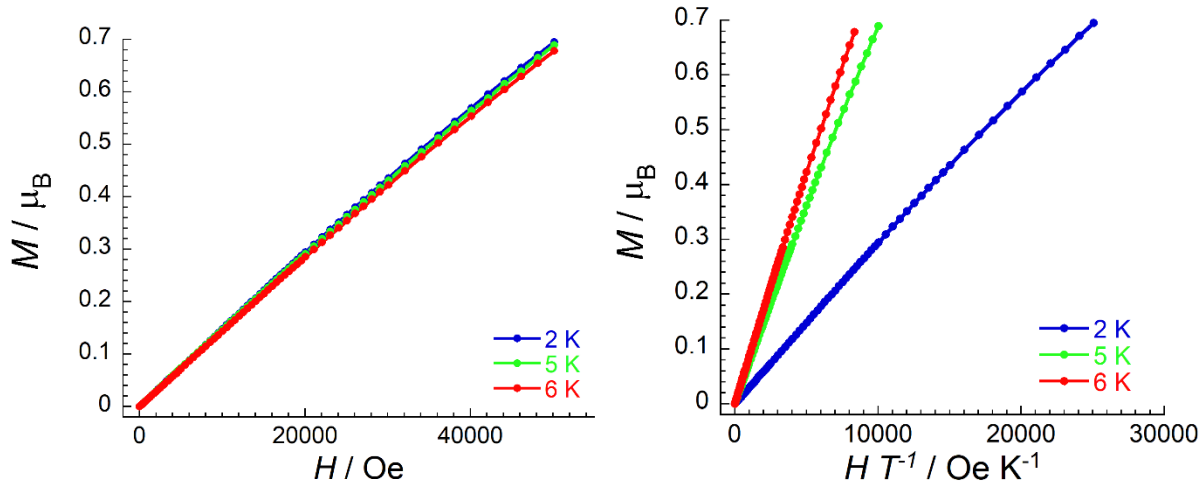

Fig. S46. Field dependence of the magnetization as *M* vs *H* (left) and *M* vs *H/T* (right) plots for **1** at 2, 5 and 6 K. The solid lines are guide for the eyes.

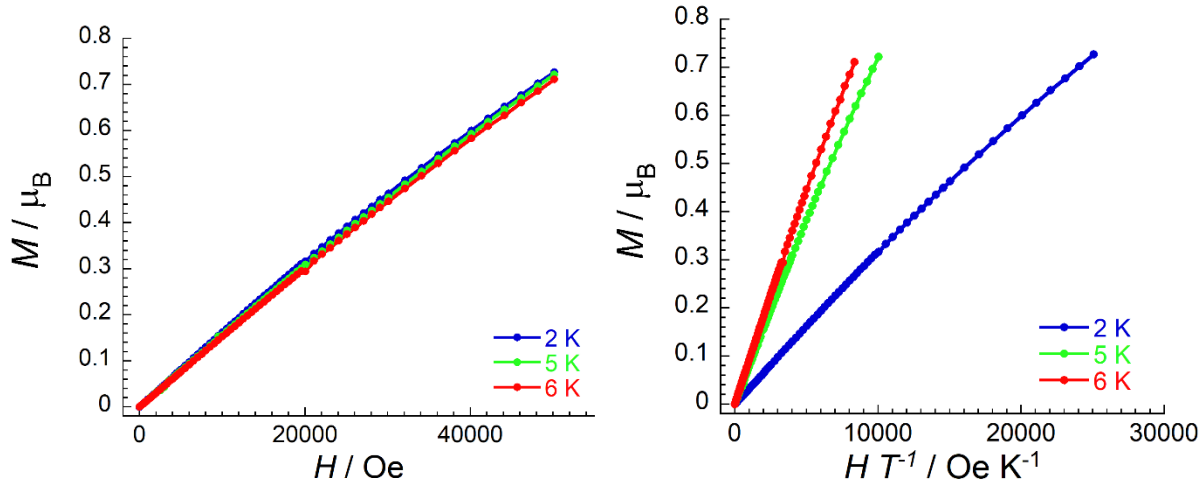

Fig. S47. Field dependence of the magnetization as *M* vs *H* (left) and *M* vs *H/T* (right) plots for **2** at 2, 5 and 6 K. The solid lines are guide for the eyes.

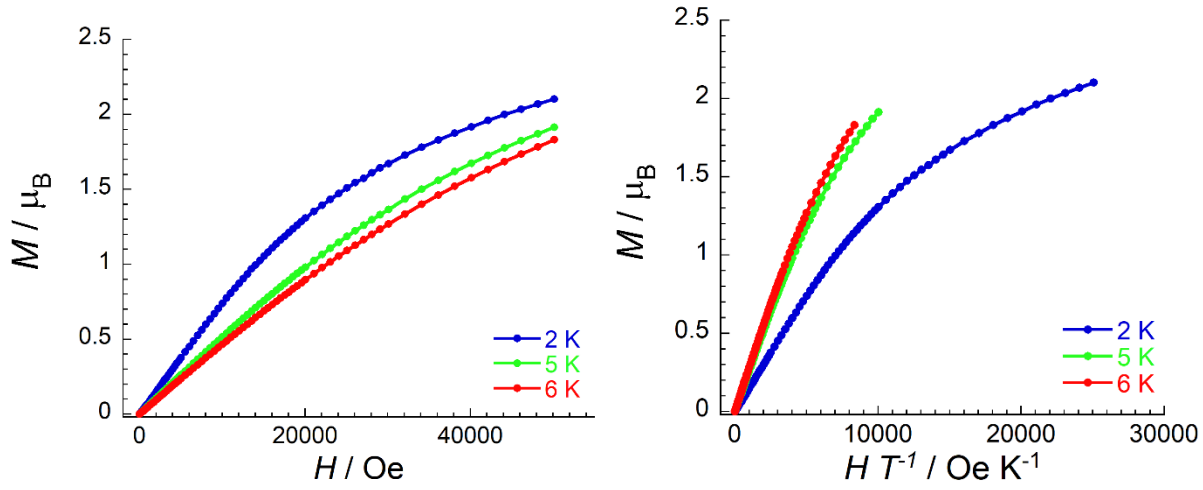

Fig. S48. Field dependence of the magnetization as *M* vs *H* (left) and *M* vs *H/T* (right) plots for **3** at 2, 5 and 6 K. The solid lines are guide for the eyes.

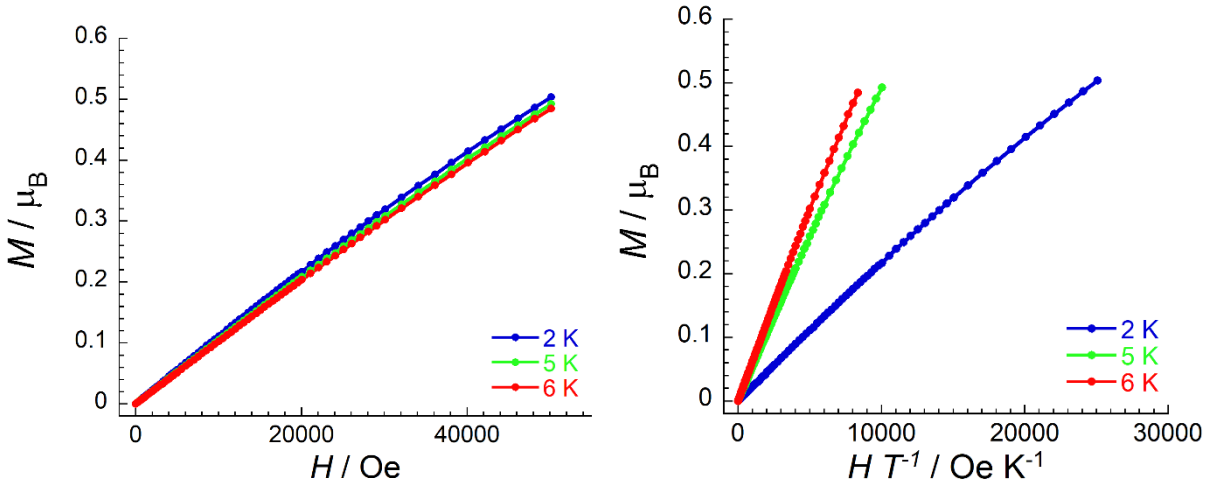

Fig. S49. Field dependence of the magnetization as *M* vs *H* (left) and *M* vs *H/T* (right) plots for **4** at 2, 5 and 6 K. The solid lines are guide for the eyes.

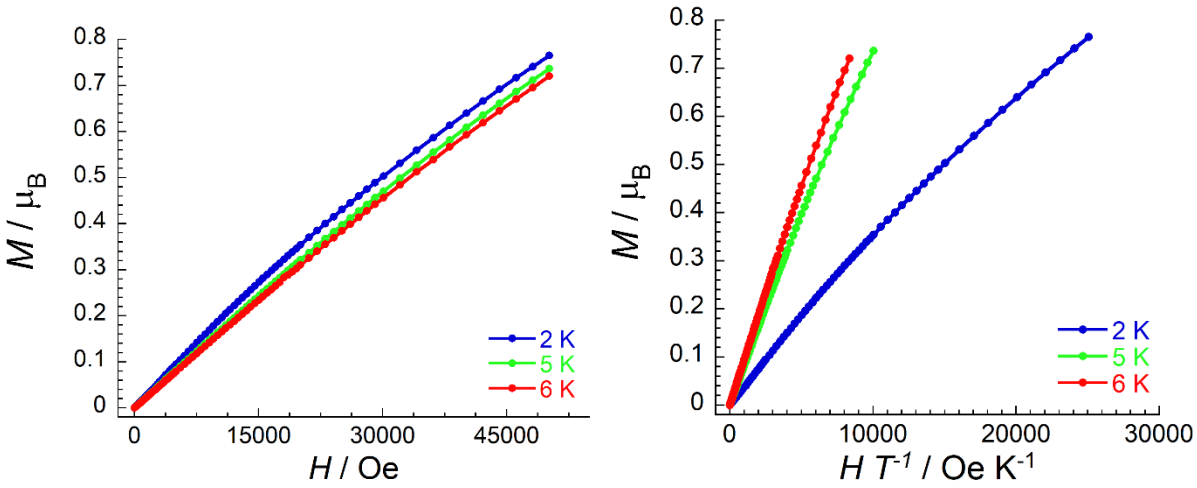

Fig. S50. Field dependence of the magnetization as *M* vs *H* (left) and *M* vs *H/T* (right) plots for **5** at 2, 5 and 6 K. The solid lines are guide for the eyes.

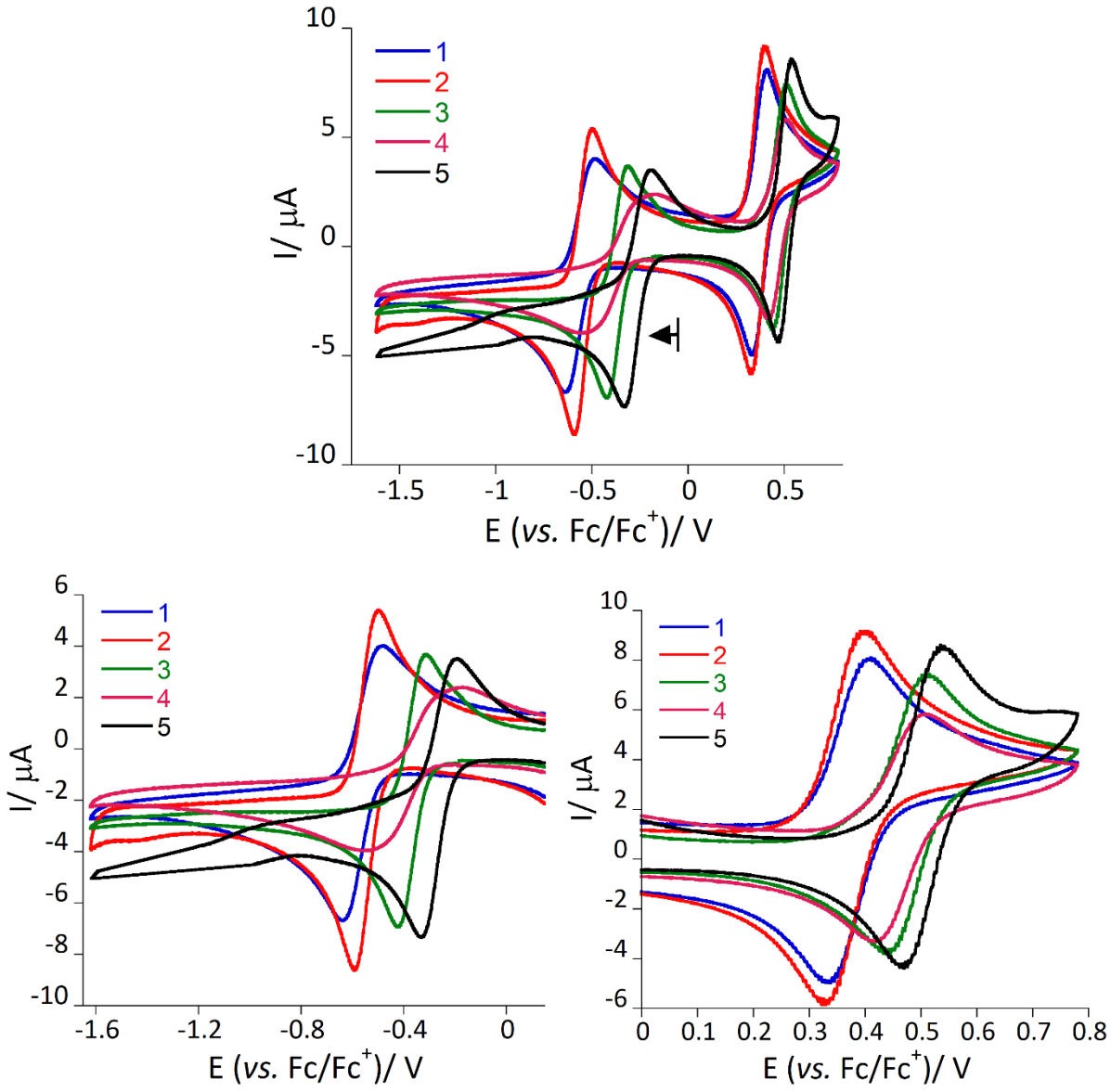

Fig. S51. Top: Cyclic voltammograms of **1** – **5** in 0.2 M (^{n}Bu$_4$N)PF$_6$ / MeCN with scan rate of 100 mV/s. Arrow indicates the direction of the potential sweep. Bottom: Zoom in section of the Cyclic voltammograms; reduction (left) and oxidation (right).

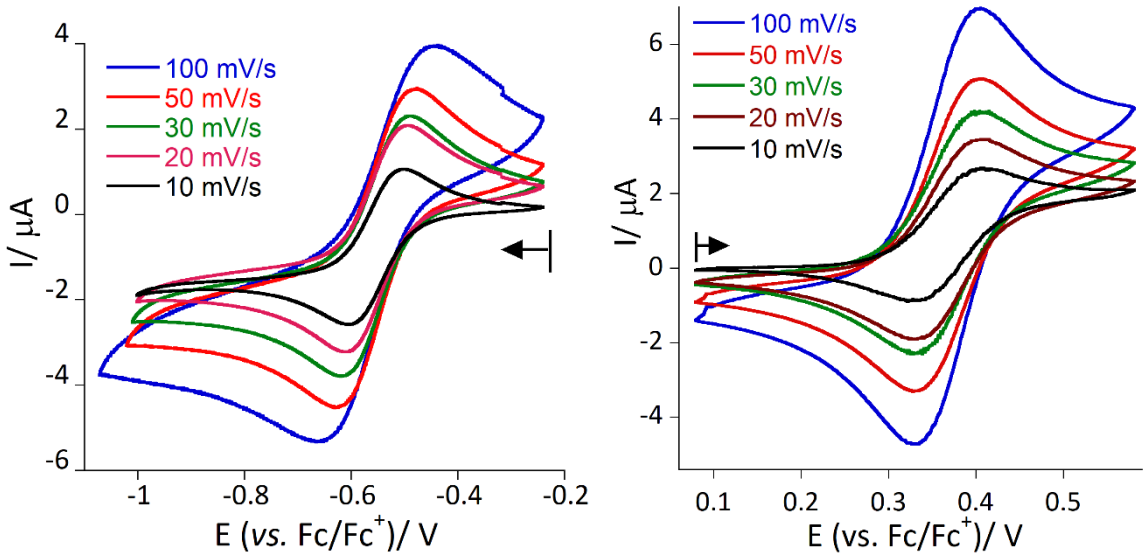

Fig. S52. Cyclic voltammograms for reduction (left) and oxidation (right) of **1** in 0.2 M (^{n}Bu$_4$N)PF$_6$ / MeCN with different scan rate. Arrow indicates the direction of the potential sweep.

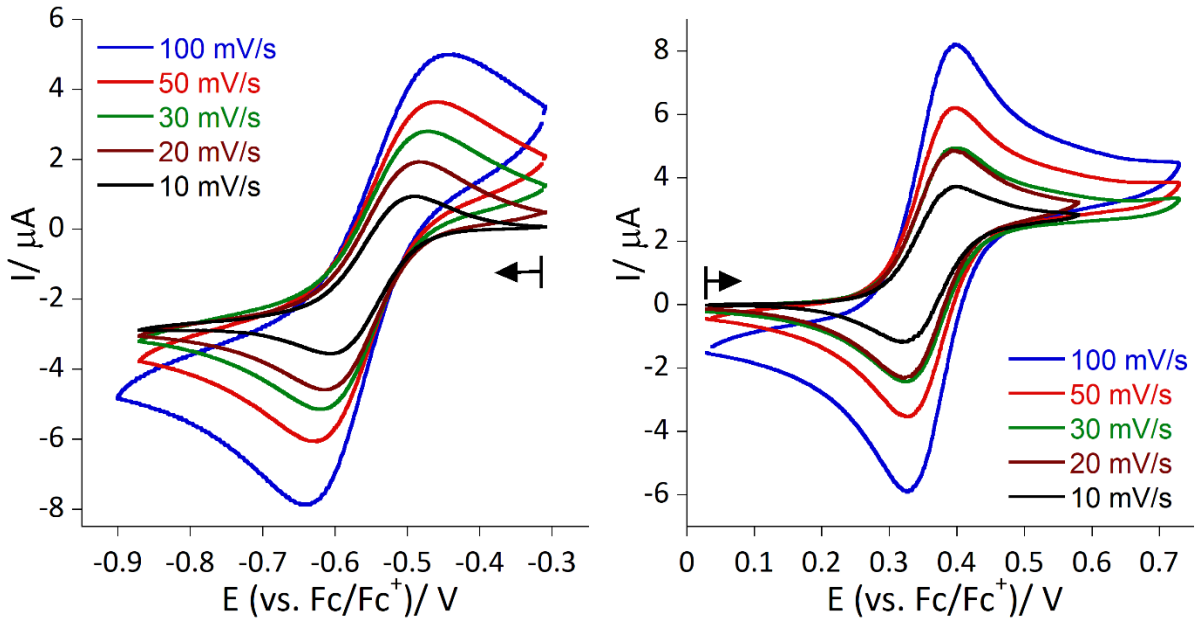

Fig. S53. Cyclic voltammograms for reduction (left) and oxidation (right) of **2** in 0.2 M (^{n}Bu$_4$N)PF$_6$ / MeCN with different scan rate. Arrow indicates the direction of the potential sweep.

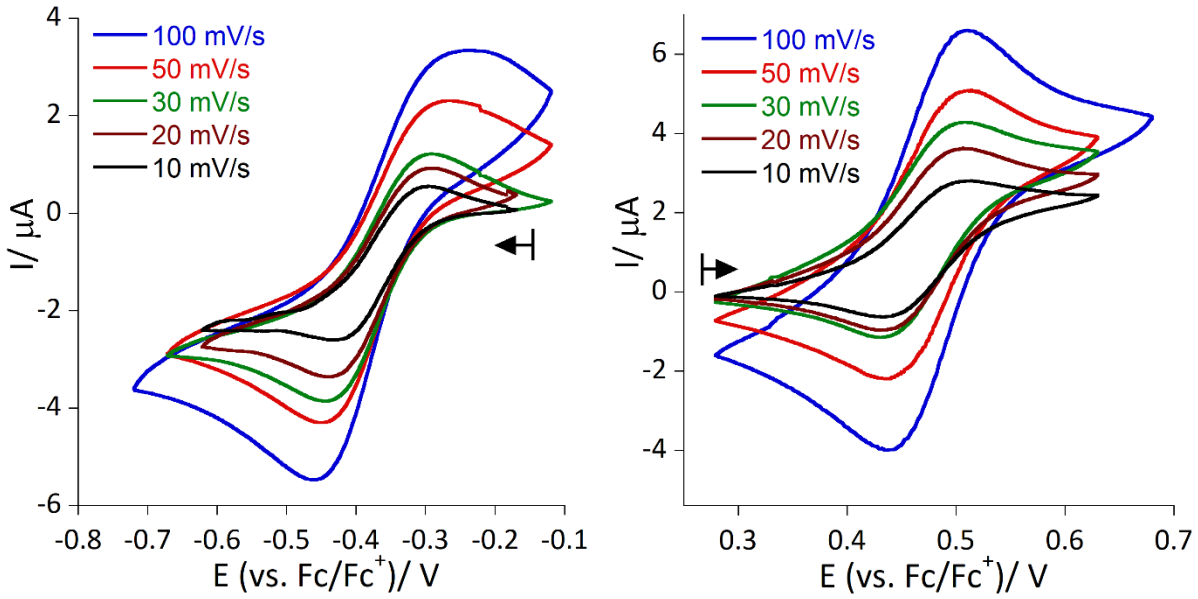

Fig. S54. Cyclic voltammograms for reduction (left) and oxidation (right) of **3** in 0.2 M (^{n}Bu$_4$N)PF$_6$ / MeCN with different scan rate. Arrow indicates the direction of the potential sweep.

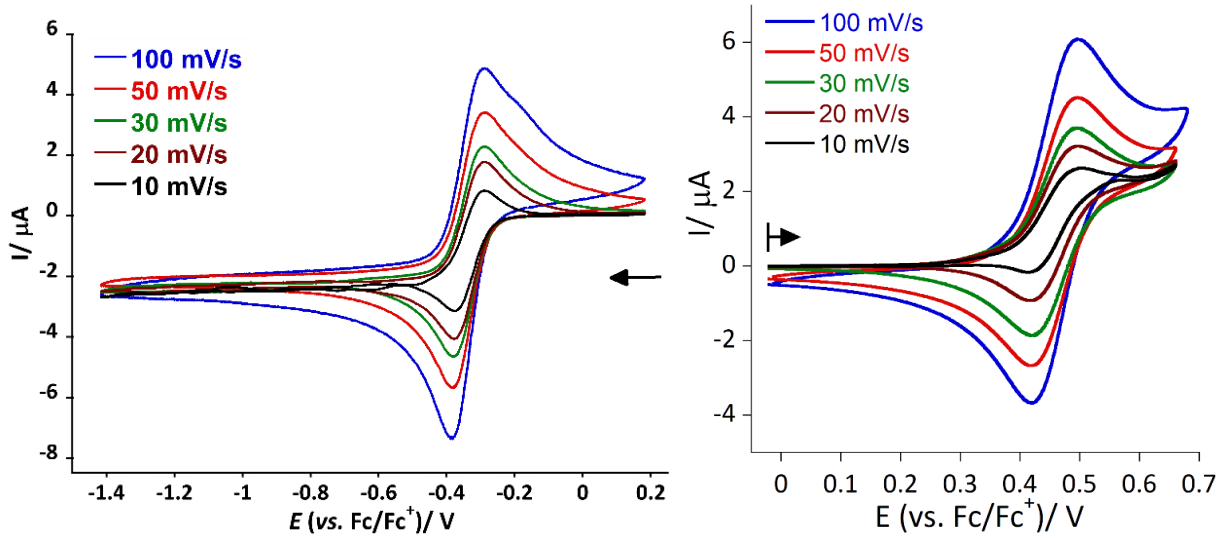

Fig. S55. Cyclic voltammograms for reduction (left) and oxidation (right) of **4** in 0.2 M (^{n}Bu$_4$N)PF$_6$ / MeCN with different scan rate. Arrow indicates the direction of the potential sweep.

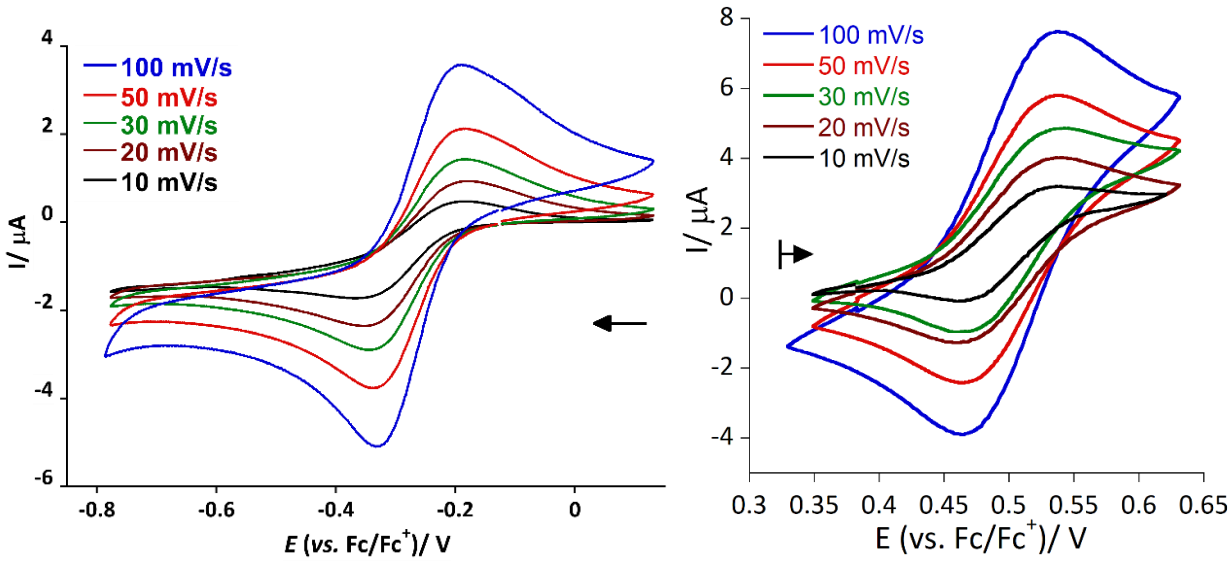

Fig. S56. Cyclic voltammograms for reduction (left) and oxidation (right) of **5** in 0.2 M (^{n}Bu$_4$N)PF$_6$ / MeCN with different scan rate. Arrow indicates the open circuit potential with the direction of the potential sweep.

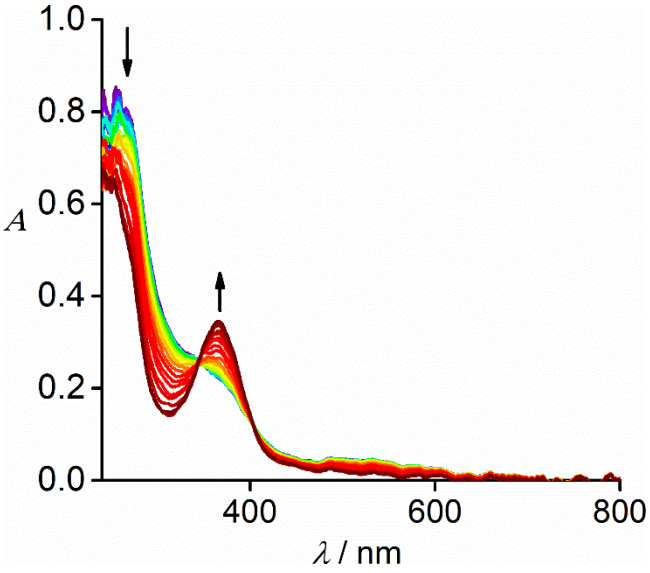

Fig. S57. Solution-state spectroelectrochemistry of **1** in 0.2 M (^{n}Bu$_4$N)PF$_6$ / MeCN over the potential range of 0.0 V to -0.65 V *vs* Fc/Fc$^+$. Arrows indicate the change in absorbance with the application of potential.

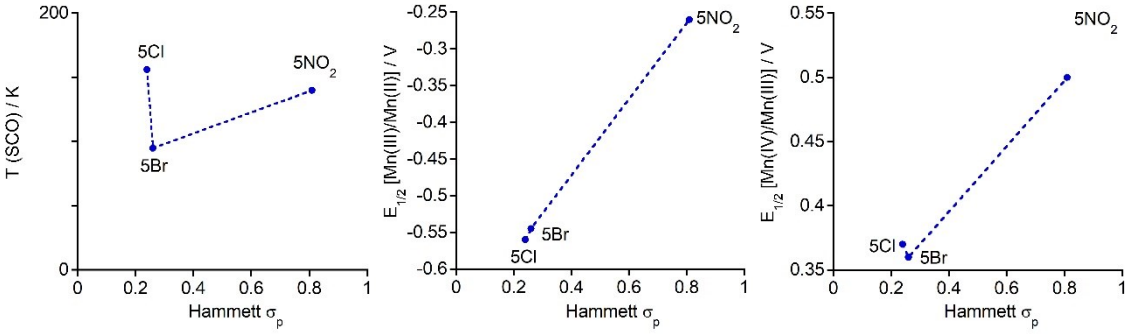

Fig. S58. Plot of T (SCO) vs Hammett σ_p, $E_{1/2}$ [Mn(III)/Mn(II)] vs Hammett σ_p, and $E_{1/2}$ [Mn(IV)/Mn(III)] vs Hammett σ_p for complexes **1** (5Cl), **2** (5Br), and **5** (5 NO_2).

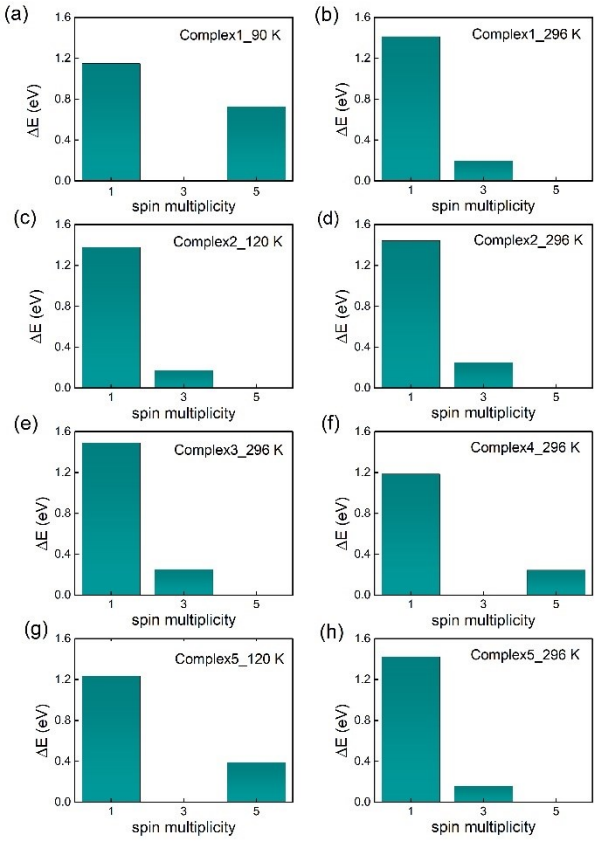

Fig. S59. The energy cost of the manganese (III) systems at different temperatures to be in spin states with multiplicity 1, 3, and 5. The triplet (spin multiplicity = 3) and quintet (spin multiplicity = 5) states are more favourable among different spin states. Temperature switches the systems from one of these two spin states to another. The preferred spin states of the systems at different temperatures are shown by the zero reference energy values, which agree well with experimental results.

Tables

Table S1. X-ray crystallography data for complexes **1** – **3**.

Complex	**1**			**2**		**3**
CCDC no	2238257	2238256	2238255	2238254	2238253	2238263
temp (K)	296	120	90	296	120	296
empirical formula	$C_{22}H_{26}N_4O_6Cl_2MnRe$	$C_{22}H_{26}N_4O_6Cl_2MnRe$	$C_{22}H_{26}Cl_2MnN_4O_6Re$	$C_{22}H_{26}Br_2MnN_4O_6Re$	$C_{22}H_{26}Br_2MnN_4O_6Re$	$C_{44}H_{48}Cl_8Mn_2N_8O_{12}Re_2$
formula wt	754.51	754.51	754.51	843.43	843.43	1646.78
cryst syst	Monoclinic	Monoclinic	Monoclinic	Monoclinic	Monoclinic	Orthorhombic
space group	$P2_1/n$	$P2_1/n$	$P2_1/n$	$P2_1/n$	$P2_1/n$	$Pbca$
a (Å)	16.6231(5)	16.5509(4)	17.0410(6)	16.8874(5)	16.5315(4)	18.4496(5)
b (Å)	9.7269(3)	9.5613(3)	9.3416(3)	9.7792(2)	9.7435(2)	17.9295(5)
c (Å)	17.4936(5)	17.3601(5)	17.2843(5)	17.5098(5)	17.5103(4)	33.6445(9)
α (deg)	90	90	90	90	90	90
β (deg)	110.7790(10)	110.9090(10)	111.2840(10)	111.050(2)	110.8880(10)	90
γ (deg)	90	90	90	90	90	90
V, Å^3	2644.58(14)	2566.29(13)	2563.82(14)	2698.69(13)	2635.10(10)	11129.3(5)
Z	4	4	4	4	4	8
d_{calcd} (g cm^{-3})	1.895	1.953	1.955	2.076	2.126	1.966
μ (mm^{-1})	5.297	5.458	5.464	7.954	8.146	5.229
F(000)	1472	1472	1472	1616	1616	6400
θ_{max} (deg)	30.597	30.738	30.619	30.595	30.557	24.216
completeness (%)	99.8	99.7	99.8	99.8	99.8	99.8
no. of. rflns collected	8116	7958	7891	8268	8047	8954
no. of. Indep rflns	5854	6194	6639	4719	6653	7009
goodness of fit on F^2	1.023	1.069	1.073	1.014	1.048	1.030
final R indices ($I>2\sigma$(I))	R1 = 0.0415 wR2 = 0.0940	R1 = 0.0510 wR2 = 0.1295	R1 = 0.0316 wR2 = 0.0675	R1 = 0.0473 wR2 = 0.1049	R1 = 0.0449 wR2 = 0.0995	R1 = 0.0287 wR2 = 0.0487
final R indices (all data)	R1 = 0.0650 wR2 = 0.1059	R1 = 0.0683 wR2 = 0.1383	R1 = 0.0434 wR2 = 0.0738	R1 = 0.1045 wR2 = 0.1287	R1 = 0.0576 wR2 = 0.1064	R1 = 0.0469 wR2 = 0.0543

Table S2 X-ray crystallography data for complexes **4** and **5**.

Complex	**4**	**5**	
CCDC no	2238262	2238260	2238261
temp (K)	296	120	296
empirical formula	$C_{22}H_{24}Br_4MnN_4O_6Re$	$C_{22}H_{26}MnN_6O_{10}Re$	$C_{22}H_{26}MnN_6O_{10}Re$
formula wt	1001.23	775.63	775.63
cryst syst	Monoclinic	Monoclinic	Monoclinic
space group	$P2_1/n$	$P2_1/c$	$P2_1/c$
a (Å)	11.3354(4)	14.4389(4)	14.5871(8)
b (Å)	19.4830(8)	9.5636(2)	9.6713(5)
c (Å)	13.7919(5)	19.3303(5)	19.4954(11)
α (deg)	90	90	90
β (deg)	97.997(2)	93.3860(10)	92.346(3)
γ (deg)	90	90	90
V, Å^3	3016.3(2)	2664.62(12)	2748.0(3)
Z	4	4	4
d_{calcd} (g cm^{-3})	2.205	1.933	1.875
μ (mm^{-1})	9.768	5.079	4.925
F(000)	1888	1520	1520
θ_{max} (deg)	30.598	30.563	30.575
completeness (%)	98.7	98.0	97.9
no. of. rflns collected	9155	8023	8231
no. of. Indep rflns	5585	6454	4422
goodness of fit on F^2	1.011	1.035	1.029
final R indices (I>2σ(I))	R1 = 0.0411	R1 = 0.0431	R1 = 0.0466
	wR2 = 0.0691	wR2 = 0.0948	wR2 = 0.0804
final R indices (all data)	R1 = 0.0929	R1 = 0.0576	R1 = 0.1231
	wR2 = 0.0810	wR2 = 0.1018	wR2 = 0.0985

Table S3. Selected bond distances (Å) and bond angles (°) in **1** and **2**.

Complex	**1**			**2**	
	296 K	120 K	90 K	296 K	120 K
Mn(1)-N(1)	2.190(4)	2.087(4)	2.048(3)	2.213(6)	2.207(5)
Mn(1)-N(2)	2.199(4)	2.101(4)	2.050(3)	2.197(6)	2.166(5)
Mn(1)-N(3)	2.092(4)	2.016(4)	1.992(3)	2.091(5)	2.121(5)
Mn(1)-N(4)	2.115(4)	2.028(4))	1.994(3)	2.115(5)	2.071(4)
Mn(1)-O(1)	1.866(3)	1.873(3)	1.876(2)	1.870(4)	1.875(3)
Mn(1)-O(2)	1.876(3)	1.878(3)	1.882(2)	1.874(4)	1.868(4)
N(1)-Mn(1)-N(2)	80.68(17)	83.68(18)	84.75(12)	79.8(2)	80.59(19)
N(1)-Mn(1)-N(3)	163.11(17)	168.91(19)	171.69(12)	85.2(2)	161.55(19)
N(1)-Mn(1)-N(4)	83.66(17)	86.34(18)	87.40(12)	160.8(2)	85.74(17))
N(1)-Mn(1)-O(1)	85.19(14)	85.28(17)	92.92(12)	95.8(2)	85.20(16)
N(1)-Mn(1)-O(2)	95.61(15)	93.61(17)	85.90(11)	85.65(19)	95.71(17)
N(2)-Mn(1)-N(3)	85.00(15)	87.42(17)	88.85(12)	162.6(2)	83.29(19)
N(2)-Mn(1)-N(4)	161.92(17)	167.90(19)	170.27(12)	85.7(2)	164.11(19)
N(2)-Mn(1)-O(1)	95.34(15)	93.39(16)	85.13(11)	95.8(2)	95.24(17)
N(2)-Mn(1)-O(2)	85.39(14)	84.86(16)	92.46(12)	112.7(2)	85.64(17)
N(3)-Mn(1)-N(4)	111.76(15)	103.24(17)	199.47(12)	87.09(18)	111.38(18)
N(3)-Mn(1)-O(1)	87.28(13)	92.58(17)	91.81(11)	92.81(13)	87.40(16)
N(3)-Mn(1)-O(2)	92.10(14))	92.15(17)	89.09(11)	91.80(19)	91.93(17)
N(4)-Mn(1)-O(1)	92.30(15)	92.58(17)	89.55(11)	92.20(19)	91.63(16)
N(4)-Mn(1)-O(2)	87.20(14)	88.98(16)	92.70(12)	86.77(18)	87.71(16)
O(1)-Mn(1)-O(2)	179.00(14)	178.03(14)	177.41(11)	178.06(18)	178.83(16)

Table S4. Selected bond distances (Å) and bond angles (°) in **3** at 296 K.

Mn(1)-N(1)	2.180(4)	Mn(2)-N(5)	2.218(4)
Mn(1)-N(2)	2.223(4)	Mn(2)-N(6)	2.225(4)
Mn(1)-N(3)	2.113(4)	Mn(2)-N(7)	2.102(4)
Mn(1)-N(4)	2.100(4)	Mn(2)-N(8)	2.086(4)
Mn(1)-O(1)	1.877(3)	Mn(2)-O(3)	1.879(3)
Mn(1)-O(2)	1.876(3)	Mn(2)-O(4)	1.873(3)
N(1)-Mn(1)-N(2)	79.96(15)	N(5)-Mn(2)-N(6)	79.11(16)
N(1)-Mn(1)-N(3)	85.94(15)	N(5)-Mn(2)-N(7)	163.34(16
N(1)-Mn(1)-N(4)	161.76(15)	N(5)-Mn(2)-N(8)	85.31(16)
N(1)-Mn(1)-O(1)	86.78(14)	N(5)-Mn(2)-O(3)	90.29(13)
N(1)-Mn(1)-O(2)	93.76(14)	N(5)-Mn(2)-O(4)	85.30(9)
N(2)-Mn(1)-N(3)	164.20(15)	N(6)-Mn(2)-N(7)	84.67(16))
N(2)-Mn(1)-N(4)	83.27(15)	N(6)-Mn(2)-N(8)	164.11(16)
N(2)-Mn(1)-O(1)	95.72(14)	N(6)-Mn(2)-O(3)	92.75(14)
N(2)-Mn(1)-O(2)	87.36(13)	N(6)-Mn(2)-O(4)	90.43(14)
N(3)-Mn(1)-N(4)	111.52(15)	N(7)-Mn(2)-N(8)	111.07(15)
N(3)-Mn(1)-O(1)	90.53(14)	N(7)-Mn(2)-O(3)	86.68(14)
N(3)-Mn(1)-O(2)	86.48(14)	N(7)-Mn(2)-O(4)	90.95(14)
N(4)-Mn(1)-O(1)	87.81(14)	N(8)-Mn(2)-O(3)	90.44(13)
N(4)-Mn(1)-O(2)	92.57(13)	N(8)-Mn(2)-O(4)	87.23(13)
O(1)-Mn(1)-O(2)	176.92(13)	O(3)-Mn(1)-O(4)	175.84(13)

Table S5. Selected bond distances (Å) and bond angles (°) in **4** and **5**.

Complex	**4**	**5**	
	296 K	296 K	120 K
Mn(1)-N(1)	2.143(4)	2.222(4)	2.119(4)
Mn(1)-N(2)	2.121(4)	2.154(4)	2.081(4)
Mn(1)-N(3)	2.052(3)	2.132(4)	2.050(4)
Mn(1)-N(4)	2.037(4)	2.066(4)	2.018(4)
Mn(1)-O(1)	1.867(3)	1.882(3)	1.892(3)
Mn(1)-O(2)	1.881(3)	1.879(3)	1.878(3)
N(1)-Mn(1)-N(2)	82.32(16)	81.27(15)	83.43(16)
N(1)-Mn(1)-N(3)	168.24(16)	162.27(15)	166.58(17)
N(1)-Mn(1)-N(4)	86.63(15)	84.57(15)	87.60(16)
N(1)-Mn(1)-O(1)	87.58(13)	86.19(14)	85.40(14)
N(1)-Mn(1)-O(2)	92.09(14)	95.70(14)	94.08(15)
N(2)-Mn(1)-N(3)	87.00(15)	83.43(15)	85.45(17)
N(2)-Mn(1)-N(4)	168.09(15)	164.02(15)	169.13(16)
N(2)-Mn(1)-O(1)	91.78(14)	95.32(15)	94.39(15)
N(2)-Mn(1)-O(2)	87.93(14)	86.66(14)	85.95(15)
N(3)-Mn(1)-N(4)	104.36(15)	111.64(14)	104.20(17)
N(3)-Mn(1)-O(1)	87.83(12)	86.38(14)	87.99(15)
N(3)-Mn(1)-O(2)	92.45(13)	92.28(14)	92.60(16)
N(4)-Mn(1)-O(1)	92.18(13)	91.08(14)	91.00(15)
N(4)-Mn(1)-O(2)	88.05(13)	87.41(14)	88.57(15)
O(1)-Mn(1)-O(2)	179.59(13)	177.46(13)	179.34(16)

Continuous Shape Measures (CShM) Analysis:

The structural distortions of the manganese(III) coordination environments were also examined by CShM using the SHAPE program (Tables 2 and S6), where a zero value of the shape factor signifies an ideal octahedral geometry.

Continuous Shape Measures (CShM) analyses were carried out to determine the geometry around the Mn ion. Based on the values obtained, the idealized polyhedron was matched with the actual coordination spheres. The smallest value is symbolic of the proximity of the actual coordination sphere and the idealized polyhedron.

Table S6: CShM analysis data for complexes **1** – **5**.

Complex	Temp.	Structure				
		HP - 6	PPY - 6	**OC - 6**	TPR - 6	JPPY - 6
1	296 K	32.092	23.489	**1.732**	9.973	26.313
	120 K	32.510	26.476	**0.714**	12.335	29.634
	90 K	32.829	27.249	**0.433**	13.385	30.933
2	296 K	32.087	22.954	**1.830**	9.832	25.797
	120 K	32.201	23.532	**1.672**	10.050	26.396
3	296 K	32.113	23.005	**1.686**	10.207	25.852
		32.391	22.441	**1.559**	11.038	25.346
4	296 K	32.543	25.522	**0.757**	12.604	28.571
5	296 K	31.934	23.185	**1.716**	9.883	26.139
	120 K	32.294	25.816	**0.817**	11.817	28.913

HP – 6: Hexagon (D6h), PPY – 6 = Pentagonal pyramid, OC – 6: Octahedron (Oh), TPR – 6: Trigonal prism (D3h), JPPY – 6 = Johnson pentagonal pyramid J2 (C5v)

Octahedral Distortion Parameters

It is well known that the center metal ion of the SCO material has been significantly distorted from a perfect octahedral geometry during the spin-state switching process, where a more regular structure can be obtained in the LS state in comparison to the HS state. This can be described by the depopulation of antibonding orbitals in the LS state. The octahedral distortion parameters (∑, Θ, ζ) have been applied to calculate the magnitude of such distortions around the manganese(III) centers using the OctaDist Program (Tables 2 and 3).[5]

∑ is the sum of the deviation from 90° of the 12 *cis*-angles of the MnN_4O_2 octahedron; Θ is the sum of the deviation from 60° of the 24 trigonal angles of the projection of the MnN_4O_2 octahedron onto the trigonal faces; ζ is the distance distortion parameter, which is the sum of deviation from individual Mn-N/O bond distances with respect to the mean metal-ligand bond distance.

Table S7 Selected Non-covalent cation-anion interactions parameters for **1** and **2**.

Complex	Type of interaction	296 K	90 K
1	N–H···O(ReO_4^-)	2.913(6) / 2.938(7) Å	2.808(5) / 2.911(4) Å
	C_{Ph}···O(ReO_4^-)	3.160(1) Å	3.166(6) Å
	C_{amine}–H···O(ReO_4^-)	3.397(7) Å	3.367(5) Å
	C_{Ph}–H···O(ReO_4^-)	3.411(7) Å	3.321(4) Å
	C_{imine}–H···Cl	3.663(6) Å	3.606(6) Å
	C_{Ph}–H···Cl	3.963(6) Å	3.846(4) Å
	Mn····Mn	8.606(1) Å	8.432(8) Å

Complex	Type of interaction	296 K	120 K
2	N–H···O(ReO_4^-)	2.923(5) / 2.948(4) Å	2.885(7) / 2.945(7) Å
	C_{Ph}···O(ReO_4^-)	3.189(5) Å	3.102(4) Å
	C_{amine}–H···O(ReO_4^-)	3.405(9) Å	3.334(5) Å
	C_{Ph}–H···O(ReO_4^-)	3.440(1) Å	3.456(4) Å
	C_{imine}–H···Br	3.716(6) Å	3.668(5) Å
	C_{Ph}–H···Br	3.981(6) Å	3.932(5) Å
	Mn····Mn	8.569(1) Å	8.532(1) Å

Table S8 Selected Non-covalent cation-anion interactions parameters for **3**.

Complex	Type of interaction	Mn(1)	Mn(2)
3	N–H···O(ReO_4^-)	3.139(5) / 3.288(5) Å	3.005(5) / 3.063(5) Å
	C_{amine}–H···O(ReO_4^-)	3.409(6) Å	3.355(6) / 3.496(7)/ 3.220(6)3.592(7) Å
	C_{Ph}–H···O(ReO_4^-)	3.536(7) / 3.573(6) Å	3.346(5) Å
	C_{imine}–H···Cl	3.818(6) Å	3.281(6) Å
	C_{Ph}···Cl	3.352(5)/ 3.420(4)	
	Cl···Cl	3.344(2) / 3.424(2) Å	3.258(2) / 3.344(2)/ 3.258(2)/ 3.424(2) Å
	Mn····Mn	8.569(1) Å	

Table S9 Selected Non-covalent cation-anion interactions parameters for **4**.

Complex	Type of interaction	296 K
4	N–H···O(ReO_4^-)	3.403(8) / 2.948(7) Å
	C_{Ph}···O(ReO_4^-)	3.206(7) Å
	C_{amine}–H···O(ReO_4^-)	3.571(6) Å
	C_{Ph}–H···O(ReO_4^-)	3.271(6) Å
	C···Br	3.493(4) Å
	C_{Ph}–H···Br	3.820(4) Å
	Br···Br	3.530(1) Å
	Mn····Mn	3.595(4) Å
		8.668(8) Å

Table S10 Selected Non-covalent cation-anion interactions parameters for **5**.

Complex	Type of interaction	296 K	120 K
5	N–H···O(ReO_4^-)	2.886(5) / 2.907(4) Å	2.876(6) / 2.863(6) Å
	C_{Ph}···O(ReO_4^-)	3.184(9)/3.178(9) Å	3.206(8)/3.128(8) Å
	C_{amine}–H···O(ReO_4^-)	3.521(7)/3.471(7) Å	3.418(7) / 3.383(7) Å
	C_{Ph}–H···O(ReO_4^-)	3.495(7) Å	3.471(7) Å
	C_{Amine}–H···O(NO_2)	4.390(7) Å	4.062(8) Å
	C_{Ph}–H···O(NO_2)	3.565(8) / 3.262(8) Å	3.533(8) / 3.286(8) Å
	Mn····Mn	8.585(1) Å	8.407(1) Å

Table S11 The energy difference between different spin states of the manganese(III) complexes at various temperature. The preferred spin states are obtained from the lowest energy.

Complex	Temperature (K)	Energy (eV)				Spin state
		Singlet	Triplet	Quintet	Septed	
1	90	1.15	0.00	0.73	3.51	Triplet
	296	1.41	0.20	0.00	2.42	Quintet
2	120	1.38	0.17	0.00	2.42	Quintet
	296	1.44	0.25	0.00	2.30	Quintet
3	296	1.49	0.25	0.00	2.37	Quintet
4	296	1.18	0.00	0.24	2.81	Triplet
5	120	1.23	0.00	0.39	3.25	Triplet
	296	1.42	0.16	0.00	2.62	Quintet

Table S12: Spin crossover behaviors of [Mn(5Cl-sal$_2$-323)](Y) (Y = counter anion) complexes with associated Mn–N/O bond distances

Complex X	$T_{1/2}$ (K)[a]	T (K)[b]	Mn–O (Å)	Mn–N (Å)	Spin State	Ref.
[Mn(5Cl-sal$_2$(323))](ReO$_4$) **Y = ReO$_4$**	T = 147 K gradual and complete	90 120 296	1.876(2)-1.882(2) 1.873(3)-1.878(3) 1.866(3)-1.876(3)	1.992(3)-2.048(3) 2.016(4)-2.101(4) 2.092(4)-2.199(4)	LS LS/HS HS	This work
[Mn(5Cl-sal$_2$-323)](BPh$_4$) **Y = BPh$_4$**	$T_{1/2}$ (1) = 168 K $T_{1/2}$ (2) = 103 K Two-step and complete	100 120 240	1.8753(13)-1.8661(13) 1.856(4)-1.864(4) 1.865(4)-1.861(4) 1.8650(19)-1.8540(19)	2.0742(18)-2.0808(16) 2.0005(17)-2.0085(17) 2.139(5)-2.121(5) 2.047(5)2.022(5) 2.098(5)-2.101(5) 2.005(5)-2.018(5) 2.167(3)-2.179(3) 2.060(2)-2.095(3)	LS HS]:[LS] (1:1) HS	[6]
[Mn(5Cl-sal$_2$-323)](TCNQ)$_{1.5}$·2MeCN **Y = TCNQ$_{1.5}$**	$T_{1/2}\downarrow$ = 73, $T_{1/2}\uparrow$ = 123; $\Delta T_{1/2}$ = 50 hysteretic and abrupt; One step and complete	100 220	1.872(2)–1.884(2) 1.871(2)–1.881(2)	2.089(3)–2.222(3) 2.095(2)–2.220(2)	HS HS	[7]
[Mn(5-Cl-Sal-323)](NO$_3$) **Y = NO$_3$**	~ 200 gradual and incomplete	100 293	1.8690(12)–1.8737(12) 1.8726(12)–1.8767(12) 1.876(2) 1.878(2)–1.879(2)	2.0695(14)–2.2613(14) 2.0628(15)–2.1929 (15) 2.091(2)–2.244(3) 2.100(3)–2.206(3)	HS HS	[8]
[Mn(5-Cl-Sal-323)]ClO$_4$ **Y = ClO$_4$**	>281 gradual and incomplete	100 260	1.8608(13) 1.8787(13) 1.8641(16)–1.8641(16) 1.8726(15)	2.1071(16)–2.2201(17) 1.9826(17)–2.0484 (18) 2.1055(19)–2.219(2)	[HS]:[LS] (1:1) HS	[8]
[Mn(5-Cl-Sal-323)]ReCl$_6$ **Y = ReCl$_6$**	gradual and incomplete	100 K 240 K 300 K	1.874(2), 1.866(2) 1.871(2), 1.866(2) 1.868(2), 1.865(2) 1.866(2), 1.864(2) 1.865(2), 1.860(2)	1.981(2), 2.046(2), 2.091(2), 2.201(2) 1.983(2), 2.053(2), 2.098(2), 2.219(2) 2.004(2), 2.080(2), 2.101(2), 2.223(2)	LS Mn(1), HS Mn(2) LS Mn(1), HS Mn(2) LS/HS Mn(1), HS Mn(2)	[9]

		353 K	1.864(2), 1.860(2)	2.039(2), 2.114(3), 2.099(2), 2.225(3)	LS/HS Mn(1), HS Mn(2)	
		403 K		2.067(2), 2.149(3) 2.097(3), 2.233(3)	LS/HS Mn(1), HS Mn(2)	
		423 K		2.071(3), 2.157(3), 2.098(3), 2.235(3)	LS/HS Mn(1), HS Mn(2)	

a: spin crossover temperature; b: structure analyses temperature; c: TCNQ = 7,7,8,8,-tetracyanoquinodimethane

Table S13: Spin crossover behaviors of [Mn(5Br-sal$_2$-323)](Y) (Y = counter anion) complexes with associated Mn–N/O bond distances

Complex X	$T_{1/2}$ (K)[a]	T (K)[b]	Mn–O (Å)	Mn–N (Å)	Spin State	Ref.
[Mn(5Br-sal2-323)](ReO4) **Y = ReO4**	$T_{1/2}$ ↑ = 96 abrupt and complete	120 296	1.868(4)-1.875(3) 1.870(4)-1.874(4)	2.071(4)-2.207(5) 2.091(5)-2.213(6)	HS/LS HS	This work
[Mn(5Br-sal$_2$-323)](BPh$_4$) **Y = BPh$_4$**	$T_{1/2}$ (1) = 164 K $T_{1/2}$ (2) = 98 K Two-step and complete	100 120 240	1.868(2)-1.876(2) 1.868(2)-1.875(2) 1.864(3)-1.867(3) 1.858(2)-1.868(2)	1.989(3)-2.061(3) 1.997(3)-2.077(3) 1.996(4)-2.081(4) 2.060(2)-2.196(2)	LS LS HS	10
[Mn(5Br-sal$_2$-323)]NO$_3$ **Y = NO$_3$**	HS	293	1.870(2)–1.875(2)	2.078(3)–2.243(3)	HS	8
[Mn(5Br-sal$_2$-323)]PF$_6$ **Y = PF$_6$**	HS	293	1.866(3)–1.878(3)	2.091(3)–2.252(4)	HS	8
[Mn(5Br-sal$_2$-323)]TCNQ$_{1.5}$·2MeCN **Y = TCNQ$_{1.5}$**	HS	100	1.871(4)–1.886(4)	2.095(5)–2.175(5)	HS	7
[Mn(5Br-sal$_2$-323)]ClO$_4$ **Y = ClO$_4$**	~ 175. Gradual [HS][HS] to [HS][LS] (1:1)	100 294	1.867 1.881 1.865(3)–1.869(3)	2.110–2.200 1.999–2.060 2.086(4)–2.184(4)	HS HS	11
[Mn(5Br-sal$_2$-323)][Ni(mnt] **Y = [Ni(mnt)$_2$]**	380. Gradual [HS](75%) to [LS]	123 296 350 400 473	1.881(3)–1.885(2) 1.869(2)–1.878(3) 1.881(3)–1.885(2) 1.881(3)–1.885(2) 1.881(3)–1.885(2)	1.984(3)–2.048(3) 2.020(3)–2.091(3) 2.031(3)–2.108(3) 2.054(3)–2.145(3) 2.065(5)–2.162(5)	LS LS Intermediate spin Intermediate spin Intermediate spin	12

[Mn(5Br-sal$_2$-323)])[Pt(mt] **Y =** [Pt(mnt)$_2$]	380. Gradual [HS](75%) to [LS]	123 296 350 400 473	1.887(4)–1.889(4) 1.876(3)–1.883(3) 1.880(3)–1.886(3) 1.874(3)–1.882(3) 1.874(3)–1.891(3)	1.975(4)–2.055(4) 2.011(4)–2.088(4) 2.025(3)–2.102(4) 2.054(4)–2.135(5) 2.054(4)–2.154(5)	LS LS Intermediate spin Intermediate spin Intermediate spin	[12]
[Mn(5Br-sal$_2$-323)][Ni(dmi] ·CH_3CN **Y =** [Ni(dmit)$_2$]	HS	296	1.866(2)-1.872(2)	2.101(3)–2.262(4)	HS	[12]
[Mn(5-Br-Sal-323)]$ReCl_6$ **Y = $ReCl_6$**	gradual and incomplete	100 K 240 K 300 K 353 K 403 K 423 K	1.871(2), 1.864(2) 1.872(2), 1.863(2) 1.873(2), 1.860(2) 1.864(2), 1.862(2) 1.862(3), 1.858(2) 1.860(3), 1.863(3)	1.985(3), 2.045(3), 2.095(3), 2.193(3) 1.989(2), 2.053(2), 2.100(2), 2.213(3) 2.014(3), 2.087(3), 2.099(3), 2.218(3) 2.046(3), 2.122(3), 2.099(3), 2.222(3) 2.069(3), 2.149(4), 2.096(3), 2.220(4) 2.072(4), 2.154(4), 2.100(4), 2.222(4)	LS Mn(1), HS Mn(2) LS Mn(1), HS Mn(2) LS/HS Mn(1), HS Mn(2) LS/HS Mn(1), HS Mn(2) LS/HS Mn(1), HS Mn(2) LS/HS Mn(1), HS Mn(2)	[9]

a: spin crossover temperature; b: structure analyses temperature

Table S14: Spin crossover behaviors of [Mn(3,5Cl-sal$_2$-323)](Y) (Y = counter anion) complexes with associated Mn–N/O bond distances

Complex X	$T_{1/2}$ (K)[a]	T (K)[b]	Mn–O (Å)	Mn–N (Å)	Spin State	Ref.
[Mn(3,5Cl-sal$_2$(323))](ReO$_4$) **Y = ReO$_4$**	$T_{1/2}$ ↑ = 104 abrupt and incomplete [HS] to [HS][LS] (1:1)	296	1.877(3)-1.876(3)	2.102(4)-2.231(5)	HS	This work
[Mn(3,5Cl-sal$_2$(323))](BPh$_4$) **Y = BPh$_4$**	$T_{1/2}$ ↓ = 139 $T_{1/2}$ ↑ = 140 ΔT= 1 K hysteretic and abrupt [HS][HS] to [HS][LS] (intermediate state) $T_{1/2}$ ↓ = 83 $T_{1/2}$ ↑ = 86 ΔT= 3 K hysteretic and abrupt [HS][LS] ~ (1:1) to [LS][LS]	250 150 115 82 10	1.869(3)-1.872(3) 1.871(2)-1.872(2) 1.866(2)-1.875(2) 1.871(4)-1.881(4) 1.874(4)-1.880(4) 1.864(4)-1.875(4) 1.864(4)-1.876(4) 1.864(10)-1.883(10) 1.876(10)-1.877(10) 1.864(10)-1.883(10) 1.876(10)-1.877(10)	2.088(3)-2.225(3) 2.079(3)-2.240(3) 2.090(3)-2.234(3) 2.017(5)-2.120(5) 2.034(5)-2.141(6) 2.081(5)-2.242(5) 2.091(5)-2.239(7) 1.967(11)-2.067(11) 1.987(12)-2.089(11) 1.967(11)-2.067(11) 1.987(12)-2.089(11)	HS HS Intermediate state LS LS	13
[Mn(3,5 Cl-sal$_2$-323)]ClO$_4$·0.5MeOH **Y = ClO$_4$**	~ 240 Gradual and incomplete	174	1.872(2)–1.877(2)	1.980(3)–2.058(3)	LS	8
[Mn(3,5Cl-sal$_2$-323)]NO$_3$·EtOH **Y = NO$_3$**	~ 260 Gradual and incomplete	293 100	1.879(19)–1.887(18) 1.8709(14)–1.8815(14)	2.013(2)–2.104(2) 1.9852(17)–2.0448(17)	Mostly LS LS	8
[Mn(3,5Cl-sal$_2$-323)]NTf$_2$ **Y = NTf$_2$**	~ 260. Gradual [HS][LS] ~ (3:1) to [HS][LS] ~ (1:1) $T_{1/2}$ ↓ = 157 $T_{1/2}$ ↑ = 171 ΔT= 14 K (5 K/ min) hysteretic and abrupt [HS][LS] ~ (1:1) to [LS]	260 210 185 120	1.881(3)–1.884(3) 1.885(2)–1.887(2) 1.8833(17)-1.8906(17) 1.8801(17)–1.8818(17) 1.888(3)	2.065(4)–2.168(4) 2.037(3)–2.132(3) 2.001(2)–2.0738(19) 2.081(2)–2.189(2) 1.993(3)–2.065(4)	Mostly HS Intermediate state Intermediate state LS	14

[Mn(3,5Cl-sal$_2$(323))](BPh$_4$) **Y = BPh$_4$**	$T_{1/2}$ = 137 Abrupt HS to HS:LS intermediate state 1 $T_{1/2}\downarrow$ = 83 $T_{1/2}\uparrow$ = 91 ΔT= 8 K (5 K/ min) hysteretic and abrupt HS:LS intermediate state 2 to LS	240 160 100	1.871(2)–1.866(2) 1.872(2)–1.864(2) 1.866(2)-1.868(2) 1.878(3)–1.869(3) 1.880(3)-1.868(3) 1.876(3)-1.858(3)	2.085(3)–2.219(3) 2.091(3)–2.228(3) 2.077(3)–2.240(3) 2.017(4)–2.088(3) 2.018(4)–2.106(4) 2.090(3)–2.111(3)	LS HS	[15]

a: spin crossover temperature; b: structure analyses temperature;

Table S15: Spin crossover behaviors of [Mn(3,5Br-sal$_2$-323)](Y) (Y = counter anion) complexes with associated Mn–N/O bond distances

Complex X	$T_{1/2}$ (K)[a]	T (K)[b]	Mn–O (Å)	Mn–N (Å)	Spin State	Ref.
[Mn(3,5Br-sal$_2$(323))](ReO$_4$) **Y = ReO$_4$**	LS	296	1.867(3)-1.881(3)	2.037(4)-2.143(4)	LS	This work
[Mn(3,5Br-sal$_2$(323))](BPh$_4$) **Y = BPh$_4$**	$T_{1/2}\downarrow$ = 86 $T_{1/2}\uparrow$ = 90 ΔT=4 K hysteretic and abrupt [HS][HS] to [HS][LS] (1:1)	240	1.858(7)-1.860(7)	2.059(9)-2.229(10)	HS	[10]
[Mn(3,5Br-sal$_2$(323))](BPh$_4$) **Y = BPh$_4$**	$T_{1/2}\downarrow$ = 82 $T_{1/2}\uparrow$ = 90 ΔT=8 K hysteretic and abrupt [HS][HS] to [HS][LS] (1:1)	25 83 110 150 250 293	1.868(14)-1.908(15) 1.903(14)-1.880(7) 1.862(15)-1.886(16) 1.904(15)-1.883(15) 1.875(7)-1.892(7) 1.880(7)-1.890(7) 1.869(7)-1.890(7) 1.884(7)-1.888(7) 1.868(2)-1.879(2) 1.874(2)-1.880(2) 1.866(3)-1.879(3) 1.874(3)-1.879(3) 1.864(3)-1.879(3) 1.866(3)-1.876(4)	2.008(18)-2.08(2) 2.064(19)-2.26(2) 2.09(2)-2.21(2) 1.98(2)-2.080(19) 2.002(8)-2.082(9) 2.081(10)-2.261(9) 2.091(10)-2.252(10) 2.018(10)-2.127(10) 2.094(3)-2.262(3) 2.078(3)-2.126(3) 2.090(4)-2.259(4) 2.076(4)-2.252(4) 2.075(5)-2.232(5) 2.079(5)-2.230(5)	HS	[16]
[Mn(3,5Br-sal$_2$-323)]ClO$_4$·½MeCN **Y = ClO$_4$**	75 Gradual and incomplete	100 200	1.873(2)–1.877(2) 1.869(2)–1.874(2)	1.984(3)–2.054(3) 2.024(3)–2.114(3)	LS LS	[17]
[Mn(3,5Br-sal$_2$-323)]BF$_4$·EtOH **Y = BF$_4$**	~175. Gradual and incomplete	100 293	1.879(3)–1.887(3) 1.869(4)–1.881(4)	1.997(5)–2.066(4) 2.053(6)–2.179(5)	LS HS	[17]
[Mn(3,5Br-sal$_2$-323)]CF$_3$SO$_3$·EtOH **Y = CF$_3$SO$_3$**	~ 200. Gradual and incomplete	100 293	1.8881(10)–1.8934(10) 1.881(2)–1.880(3)	1.9863(12)–2.0569(12) 2.053(3)–2.166(4)	LS HS	[17]

[Mn(3,5Br-sal$_2$-323)]ClO_4·EtOH **Y = ClO_4**	>200. Gradual and incomplete	100 293	1.870(4)–1.8888(4) 1.868(3)–1.882(3)	2.0009(5)–2.098(5) 2.063(5)–2.200(4)	LS HS	[17]
[Mn(3,5Br-sal$_2$-323)]NO_3·EtOH **Y = NO_3**	>250. Gradual and incomplete	100	1.8820(16)–1.8831(16)	1.982(2)–2.045(2)	LS	[17]
[Mn(3,5Br-sal$_2$-323)]PF_6 ½·MeOH **Y = PF_6**	LS	100	1.861(2)–1.879(2)	1.980(3)–2.058(3)	LS	[17]

a: spin crossover temperature; b: structure analyses temperature;

Table S16: Spin crossover behaviors of [Mn(5NO_2-sal_2-323)](Y) (Y = counter anion) complexes with associated Mn–N/O bond distances

Complex X	$T_{1/2}$ (K)[a]	T (K)[b]	Mn–O (Å)	Mn–N (Å)	Spin State	Ref.
[Mn(5NO_2-sal_2(323))](ReO_4) **Y = ReO_4**	T = 115 Gradual and complete	120 296	1.878(3)–1.892(3) 1.879(3)- 1.882(3)	2.018(4)–2.119(4) 2.066(4)–2.222(4)	LS HS	This work
[Mn(5NO_2-sal_2(323))](AsF_6) **Y = AsF_6**	$T_{1/2}$ ↑ = 317 gradual [HS][HS] to [HS][LS] (1:1) $T_{1/2}$ ↑ = 164 gradual [HS][LS] (1:1) to [LS][LS]	100 300	1.881(5)-1.882(5) 1.891(4)-1.891(5) 1.874(5)-1.892(5) 1.891(4)-1.892(5)	1.992(6)-2.065(7) 1.983(5)-2.044(6) 2.043(6)-2.220(7) 2.010(6)-2.090(6)	LS LS Intermediate state Intermediate state	[18]
[Mn(5NO_2-sal_2(323))](SbF_6) **Y = SbF_6**	$T_{1/2}$ ↑ = 305 gradual $T_{1/2}$ ↑ = 131 gradual [HS][HS] to [HS][LS] (1:1)	100 300	1.882(3)-1.892(3) 1.892(3)-1.894(3) 1.867(4)-1.883(4) 1.877(4)-1.881(4)	2.023(4)-2.184(4) 1.992(4)-2.052(4) 2.035(5)-2.216(6) 2.007(5)-2.083(5)	LS LS Intermediate state Intermediate state	[18]
[Mn(5NO_2-sal_2-323)]BF_4·3H_2O **Y = BF_4**	HS	300	1.874(5)-1.892(5) 1.891(4)-1.892(5)	2.080(4)-2.258(5) 2.000(4)-2.106(5)	LS HS	[18]
[Mn(5NO_2-sal_2-323)]NO_3·MeCN·0.5H_2O **Y = NO_3**	~ 200. Gradual and incomplete mostly HS to [HS][LS] (1:1)	100 293	1.898–1.898 1.872–1.878 1.942–1.957 1.871-1.875	1.999–2.047 2.080–2.241 2.018–2.121 2.105–2.234	Intermediate state mostly HS	[19]
[Mn(5NO_2-sal_2-323)]ClO_4·MeCN·0.5H_2O **Y = ClO_4**	< 200. Gradual and incomplete mostly HS to [HS][LS] (1:1)	100 260	1.893–1.899 1.870–1.876 1.908–1.919 1.875–1.884	1.987–2.046 2.063–2.269 2.014–2.073 2.018–2.269	Intermediate state mostly HS	[19]
[Mn(5NO_2-sal_2-323)]ClO_4·0.5MeCN·0.5H_2O **Y = ClO_4**	HS	100	1.873-1.875	2.103-2.272	HS	[19]

[Mn(5NO_2-sal$_2$-323)]PF_6 **Y = PF_6**	LS	100	1.882–1.891 1.882–1.883	1.984–2.046 1.990–2.2061	LS	[19]
[Mn(5NO_2-sal$_2$-323)]OTf **Y = OTf**	mostly HS	100	1.864–1.887	2.049–2.241	mostly HS	[19]
[Mn(5NO_2-sal$_2$-323)]BPh_4 **Y = BPh_4**	HS	100	1.872–1.877	2.083–2.278	HS	[19]

a: spin crossover temperature; b: structure analyses temperature;

Table S17: Spin crossover behaviors of [Mn(X-sal$_2$-323)]ReO_4 (X= ligand substituents) complexes with associated Mn–N/O bond distances

Complex	$T_{1/2}$ (K)[a]	T (K)[b]	Mn–O (Å)	Mn–N (Å)	Spin State	Ref.
[Mn(5Cl-sal$_2$(323))](ReO$_4$)	T = 147 K gradual and complete	90 120 296	1.876(2)-1.882(2) 1.873(3)-1.878(3) 1.866(3)-1.876(3)	1.992(3)-2.048(3) 2.016(4)-2.101(4) 2.092(4)-2.199(4)	LS LS/HS HS	This work
[Mn(5Br-sal2-323)](ReO4)	$T_{1/2}\uparrow$ = 96 abrupt and complete	120 296	1.868(4)-1.875(3) 1.870(4)-1.874(4)	2.071(4)-2.207(5) 2.091(5)-2.213(6)	HS/LS HS	This work
[Mn(3,5Cl-sal$_2$(323))](ReO$_4$)	$T_{1/2}\uparrow$ = 104 abrupt and incomplete [HS] to [HS][LS] (1:1)	296	1.877(3)-1.876(3)	2.102(4)-2.231(5)	HS	This work
[Mn(3,5Br-sal$_2$(323))](ReO$_4$)	LS	296	1.867(3)-1.881(3)	2.037(4)-2.143(4)	LS	This work
[Mn(5NO$_2$-sal$_2$(323))](ReO$_4$)	T = 115 Gradual and complete	120 296	1.878(3)–1.892(3) 1.879(3)- 1.882(3)	2.018(4)–2.119(4) 2.066(4)–2.222(4)	LS HS	This work
[Mn(5H-sal$_2$-323)](ReO$_4$)	84 ΔT= 1 K hysteretic and abrupt [HS][LS] (5:3) to Intermediate spin state $T_{1/2}\downarrow$ = 71 $T_{1/2}\uparrow$ = 77 ΔT= 6 K hysteretic and abrupt Intermediate spin state to LS	10 80 100 250	1.878(12)–1.884(12) 1.872(12)–1.871(1) 1.878(8)–1.874(8) 1.875(8)–1.878(9) 1.875(9)–1.885(9) 1.860(9)–1.869(9) 1.875(4)–1.872(4) 1.879(4)–1.868(4)	1.991(14)-2.079(13) 1.975(13)-2.062(14) 2.051(11)-2.148(10) 2.020(12)-2.129(11) 1.986(10)-2.066(10) 2.065(9)-2.237(10) 2.049(4)-2.163(5) 2.067(5)-2.213(5)	LS Intermediate state Intermediate state mostly HS	[20]**

Please note during our manuscript preparation one Mn(III) system without any substitution on salicylaldehyde ligand [Mn(X-sal$_2$-323)](ReO$_4$) (X = 5-H,) was published by Dobbelaar *et al* (*Angew. Chem. Int. Ed.* ***2022**, 61, e202114021,* reference no 19).

References

1. T. Degen, M. Sadki, E. Bron, U. König and G. Nénert, *Powder Diffr.*, 2014, **29**, S13-S18.
2. G. M. Sheldrick, SADABS Version 2.03, Bruker Analytical X-Ray Systems, Madison, WI, USA, 2000.
3. O. V. Dolomanov, L. J. Bourhis, R. J. Gildea, J. A. K. Howard and H. Puschmann, *J. Appl. Crystallogr.*, 2009, **42**, 339-341.
4. C. F. Macrae, P. R. Edgington, P. McCabe, E. Pidcock, G. P. Shields, R. Taylor, M. Towler and J. van de Streek, *J. Appl. Crystallogr.*, 2006, **39**, 453-457.
5. R. Ketkaew, Y. Tantirungrotechai, P. Harding, G. Chastanet, P. Guionneau, M. Marchivie and D. J. Harding, *Dalton Trans.*, 2021, **50**, 1086-1096.
6. S. Ghosh, S. Bagchi, M. Das, S. Kamilya and A. Mondal, *Dalton Trans*, 2020, **49**, 14776-14780.
7. A. V. Kazakova, A. V. Tiunova, D. V. Korchagin, G. V. Shilov, E. B. Yagubskii, V. N. Zverev, S. C. Yang, J. Y. Lin, J. F. Lee, O. V. Maximova and A. N. Vasiliev, *Chemistry*, 2019, **25**, 10204-10213.
8. B. Gildea, L. C. Gavin, C. A. Murray, H. Muller-Bunz, C. J. Harding and G. G. Morgan, *Supramol Chem*, 2012, **24**, 641-653.
9. A. V. Tiunova, A. V. Kazakova, D. V. Korchagin, G. V. Shilov, S. M. Aldoshin, A. I. Dmitriev, M. V. Zhidkov, K. V. Zakharov and E. B. Yagubskii, *Journal*, 2022, **23**.
10. S. Ghosh, S. Bagchi, S. Kamilya and A. Mondal, *Dalton Trans*, 2021, **50**, 4634-4642.
11. S. Wang, M. Ferbinteanu, C. Marinescu, A. Dobrinescu, Q. D. Ling and W. Huang, *Inorg. Chem.*, 2010, **49**, 9839-9851.
12. Y. Chen, F. Cao, R. M. Wei, Y. Zhang, Y. Q. Zhang and Y. Song, *Dalton Trans*, 2014, **43**, 3783-3791.
13. V. B. Jakobsen, E. Trzop, E. Dobbelaar, L. C. Gavin, S. Chikara, X. Ding, M. Lee, K. Esien, H. Müller-Bunz, S. Felton, E. Collet, M. A. Carpenter, V. S. Zapf and G. G. Morgan, *J. Am. Chem. Soc.*, 2022, **144**, 195-211.
14. A. J. Fitzpatrick, E. Trzop, H. Muller-Bunz, M. M. Dirtu, Y. Garcia, E. Collet and G. G. Morgan, *Chem Commun (Camb)*, 2015, **51**, 17540-17543.
15. A. V. Tiunova, A. V. Kazakova, D. V. Korchagin, G. V. Shilov, L. V. Zorina, S. V. Simonov, K. V. Zakharov, A. N. Vasiliev and E. B. Yagubskii, *Chemistry*, 2021, **27**, 17609-17619.
16. V. B. Jakobsen, E. Trzop, L. C. Gavin, E. Dobbelaar, S. Chikara, X. Ding, K. Esien, H. Muller-Bunz, S. Felton, V. S. Zapf, E. Collet, M. A. Carpenter and G. G. Morgan, *Angew. Chem. Int. Ed.*, 2020, **59**, 13305-13312.
17. K. Pandurangan, B. Gildea, C. Murray, C. J. Harding, H. Muller-Bunz and G. G. Morgan, *Chem. Eur. J.*, 2012, **18**, 2021-2029.
18. S.-Z. Zhao, Z.-M. Yu, C.-Y. Qin, P.-Y. Xu, Y.-T. Wang, Y.-H. Li and S. Wang, *Inorganica Chimica Acta*, 2022, **538**.
19. I. A. Kühne, L. C. Gavin, M. Harris, B. Gildea, H. Müller-Bunz, M. Stein and G. G. Morgan, *J. Appl. Phys.*, 2021, **129**.
20. E. Dobbelaar, V. B. Jakobsen, E. Trzop, M. Lee, S. Chikara, X. Ding, H. Müller-Bunz, K. Esien, S. Felton, M. A. Carpenter, E. Collet, G. G. Morgan and V. S. Zapf, 2022, **61**, e202114021.